TEAM Hub
Tissue Engineering & Applied Materials

1st Tissue Engineering and Applied Materials (TEAM) Hub Workshop

Trainees Abstracts

June 26-28, 2023

1st TEAM Hub Workshop
Ottawa, ON
June 26-28, 2023

TEAM Hub
Tissue Engineering & Applied Materials

Harnessing 3D bioprinting to strengthen cancer stem cell-targeting drug discovery

Veronika Yevdokimova[1,2], Christopher J. Bergin[2], Amanda M. da Silva[2], Jacob L. Billingsley[1,2], and Yannick D. Benoit[2]

[1] Ph.D. program in Cellular and Molecular Medicine, Faculty of Medicine, University of Ottawa, Canada.
[2] Department of Cellular and Molecular Medicine, Faculty of Medicine, University of Ottawa, Canada.

Introduction

Cancer stem cells (CSCs) represent a rare and dynamic constituent of tumor cellular heterogeneity, holding self-renewal and tumor-initiation functions. CSCs are the root of cancer and play a central role in disease recurrence and acquired therapeutic resistance [1]. The development of CSC-targeting drugs constitutes a substantial challenge due to the importance of several molecular networks shared between neoplastic stemness and healthy pools of stem cells. Thus, phenotypic drug screening approaches are best suited to identify context-specific compounds that disrupt CSC functions while exerting minimal impact on healthy stem cells [2]. Our group recently developed a serial 3D organoid formation assay to evaluate the potential of experimental compounds to block CSC functions *ex vivo* [3]. Such a method helped identify compounds altering epigenetic and pluripotency networks essential to human colorectal CSCs [4, 5]. Emerging 3D bioprinting technology enables miniaturization and increased throughput of organoid formation assays measuring clonogenic capacities in tissue samples.

Methodology

Using a temperature-controlled basement membrane extract bioprinter, we adapted our serial 3D organoid formation assay to perform rapid and cost-efficient drug screening experiments. Specifically, we used 24 and 96-well culture plates to print mini domes of basement membrane extracts containing fragments of patient-derived colorectal tumors or healthy colonic mucosa. We used this system to compare the efficacy of various chemical entities to block clonogenic functions in primary colorectal tumor organoids versus healthy colonic organoids. Such a bioprinting process was also valuable in generating miniaturized organoid cultures from human pluripotent stem cells and standard immortalized lines for screening purposes. Moreover, we combined this bioprinting process with a CRISPR knock-in reporter system, tracing the expression of the colon CSC marker LGR5 in primary tumor tissues to evaluate the impact of drug treatments on CSC frequency within colorectal tumor organoids [6].

Results

We demonstrated the power of the above-described pipeline with different applications:

1) We screened a collection of 68 epigenetic probes from the Structural Genomic Consortium to identify chromatin-regulating pathways mediating tumor-initiating functions in colorectal tumor tissues.
2) We validated the efficacy of repurposed drugs, initially identified as pluripotency disruptors in stem cell-based phenotypic screening, to block tumor initiation, self-renewal, and CSC marker expression in colorectal tumor organoids.
3) We confirmed the selective toxicity of a compound inhibiting the expression of the histone methyltransferase G9a (YB-1471) toward colorectal tumor organoids vs. healthy colonic organoids. The anti-CSC effects of this compound were confirmed *in vivo*, through serial tumor transplantations assays.

Conclusions

Organoid formation assays supported by 3D bioprinting technology represent a significant opportunity for phenotypic drug screening campaigns through its versatility, superior reproducibility, the prospect of increased throughput, and the diversity of model applications and readouts.

Acknowledgements

The Structural Genomic Consortium, Corning Inc., the Global Tissue Consenting initiative, CRS, and CIHR.

References

1. Haebe JR, Bergin CJ, Sandouka T, Benoit YD. Emerging role of G9a in cancer stemness and promises as a therapeutic target. *Oncogenesis* 2021; 10: 76.
2. Benoit YD. Identification of Novel Molecules Targeting Cancer Stem Cells. *Methods Mol Biol* 2018; 1765: 333-347.
3. Bergin CJ, Benoit YD. Protocol for serial organoid formation assay using primary colorectal cancer tissues to evaluate cancer stem cell activity. *STAR Protoc* 2022; 3: 101218.
4. Bergin CJ, Zouggar A, Haebe JR, Masibag AN, Desrochers FM, Reilley SY *et al*. G9a controls pluripotent-like identity and tumor-initiating function in human colorectal cancer. *Oncogene* 2021; 40: 1191-1202.
5. Masibag AN, Bergin CJ, Haebe JR, Zouggar A, Shah MS, Sandouka T *et al*. Pharmacological targeting of Sam68 functions in colorectal cancer stem cells. *iScience* 2021; 24: 103442.
6. Shimokawa M, Ohta Y, Nishikori S, Matano M, Takano A, Fujii M *et al*. Visualization and targeting of LGR5. *Nature* 2017; 545: 187-192.

1st TEAM Hub Workshop
Ottawa, ON
June 26-28, 2023

TEAM Hub
Tissue Engineering & Applied Materials

Monocyte infiltration and hybrid subpopulation of tumour-associated macrophages drive early vaccinia-mediated B16-F12 tumour reduction

D. Ahmed[1], R. Skillings[1], O. Abdo[1], A. Fareghdeli[2], Z. Versey[1,2], L. Guidolin[2], E. Cassol[1]

[1]Department of Health Sciences, Carleton University, Ottawa, Canada
[2]Department of Systems and Computer Engineering, Carleton University, Ottawa, Canada

Introduction

Oncolytic viruses (OVs) are a potent therapeutic in the fight against cancers[1]. They are capable of selectively killing cancer cells as well as inducing local and systemic inflammation to re-engage anti-tumour immunity[1]. Vaccinia virus (VACV) is a promising OV candidate currently part of several clinical trials[2] but to unlock its immunomodulatory potential, a thorough understanding of how VACV modulates the tumour microenvironment (TME) is required.

Tumour-associated macrophages (TAMs) represent up to 50% of stromal cells in the TME[3] and play a critical role in establishing the favourable immunosuppressive conditions required for optimal tumour growth[4]. Yet, these cells are key to therapeutic responses to other immunotherapies such as checkpoint inhibitors and TAM-depleting strategies[3,4]. Emerging evidence suggests that OVs can reprogram TAM function towards a more pro-inflammatory phenotype[4]. Yet, the precise mechanisms outline this reprogramming has yet to be elucidated.

Methodology

To evaluate how VACV alters TAM frequency and phenotype *in vivo*, we implanted B16-F10 melanoma cells ($2x10^6$ cells in PBS mixed with Matrigel) subcutaneously into 3-month-old C57BL/6J mice. When tumours reach a volume of 50-75mm^3, they were injected with either PBS or a 1e7 PFU solution of a mouse adapted VACV strain (Western Reserve). Mice were harvested 24hrs after each treatment and 5 days after the completion of the treatment regimen. Tumours and spleens will be digested and the relative frequencies of monocytes, T cells, and TAM subpopulations is evaluated *via* flow cytometry using panels of linage specific markers.

Results

In the early phase of the treatment regimen, there are minimal changes within the local tumour microenvironment and the spleen in the presence of VACV, with a no change in splenic subpopulations and a small increase in immune cells, due to increased inflammatory monocyte infiltration. This is accompanied by decreased percentage of M2-like late TAMs, which are primary drivers of the immunosuppressive TME. In addition, the TAMs present possessed increased M1 marker CD80, indicating an inflammatory shift within the tumour. Splenic enlargement is evident after the second VACV injection, with increased splenic inflammatory monocytes. The reduction in tumour size after the second injection is linked to further inflammatory monocyte infiltration and decreased in the late TAM population. In addition, TAM shifted away from expressing CD80 into a more hybrid phenotype, expressing the M1 marker CD86 and M2 marker CD206. Increased CD8+ T cell and inflammatory monocyte levels in the spleen and the tumour is evident 24hrs after the third VACV injection. This is also associated with increased early TAM population and decreased late TAM population, suggesting an inflammatory shift. Yet, the TAMs continued to possess the hybrid CD86/CD206 phenotype. Five days after the final injection further establishes the presence of inflammatory monocyte and CD8+ T cells in the spleen and tumour, as well as the early TAM population within the tumour.

Conclusions

In summary, the reduction in tumour size in the early phase of VACV treatment regimen is linked to increased inflammatory monocyte infiltration and decreased late TAM population, followed by increased early TAM population that possess a hybrid M1/M2 phenotype before the activation and influx of CD8+ T cells. This demonstrates that myeloid cell populations are the primary drivers of VACV-mediated anti-tumour response. Further work is required to outline their specific contributions to the overall response.

Acknowledgements

This research was done in collaboration with Turnstone Biologics, who provided the VACV used in this study.

References

1. Cao, G-D, H, X-B, Sun, Q., Chen, S., Wan, K., Xin, X., Feng, X., Li, P-P, Chen, B., Xiong, M-M. "The Oncolytic Virus in Cancer Diagnosis and Treatment" Front Oncol, Vol 10, 2020
2. Al Yaghchi, C., Zhang, Z., Alusi, G., Lemoine, N.R., Wang, Y. "Vaccinia virus, a promising new therapeutic agent for pancreatic cancer" Immunotherapy, Vol 7, Issue 12, pp. 1249-1258, 2015
3. Li, M., He, L., Zhu, J., Zhang, P., Liang, S. "Targeting tumor-associated macrophages for cancer treatment" BMC Cell Biosci, Vol. 12, Issue 85, 2022.
4. Petty, A.J., Owen, D.H., Yang, Y., Huang, X. "Targeting Tumor-Associated Macrophages in Cancer Immunotherapy" Cancers (Basel), Vol. 13, Issue 21, pp. 5318, 2021.

1st TEAM Hub Workshop
Ottawa, ON
June 26-28, 2023

Unveiling the complexity of tumour-associated macrophages: insights from *in vitro* and *in vivo* models

Skillings R[1], Ahmed D[1], Boxma A[1], Abdo O[1], Fareghdeli A[2], Versey Z[1], Mejlaoui R[1], Sheridan M-E[1], Al Daraawi M[1], Guidolin L[2], Cassol E[1]

[1]Department of Health Sciences, Carleton University and [2]Department of Systems and Computer Engineering, Carleton University

Introduction

Tumour-associated macrophages (TAMs) are innate immune cells highly present within the tumour that can either promote tumour growth and immunosuppression **(M2-like TAMs)** or fight tumours and initiate anti-tumour immunity **(M1-like TAMs)** [1]. **Vaccinia virus (VACV)** is an oncolytic virus that infects and kills tumour cells and induces strong anti-tumour immunity [2]. Recent studies have found that **VACV is capable of reprogramming M2-like TAMs towards an M1-like phenotype** [1]. However, the mechanisms underlying this TAM reprogramming are not well known**.** Understanding these mechanisms could be used to improve the immunotherapeutic potential of VACV.

Methodology

To study VACV-dependent TAM reprogramming *in vitro*, we first needed to establish an *in vitro* TAM model and compare the TAM phenotype to its *in vivo* counterpart. Transwell and direct co-culture *in vitro* TAM models were developed by co-culturing murine bone marrow derived macrophages (BMDMs) with murine melanoma B16-F10 tumour cells. In the transwell model, B16-F10 cells seeded on 0.4 µm pore transwell inserts were added to BMDM cultures with or without IL-4/IL-10 cytokines. In the direct model, B16-F10 cells were seeded directly on top of BMDM cultures. In both models, cells were co-cultured for 24-72h before supernatants were collected for IL-10 cytokine analysis and TAMs were phenotyped via flow cytometry analysis. To establish the relevant *in vivo* TAM phenotype, B16-F10 tumours were first engrafted onto young female C57BL/6 mice. At days 1-, 3-, 5-, and 10-days post-engraftment, tumours were harvested, digested and the TAMs were phenotyped via flow cytometry analysis.

Results

Overall, we found that B16-F10 TAMs existed in mixed M1/M2, M2-like and M1-like subpopulations both *in vivo* and *in vitro*. In the *in vivo* model, we observed a general increase in M2-like/pro-tumourigenic TAM marker expression and M2-like TAM subpopulations as the B16-F10 tumours grow over time. Interestingly, the *in vitro* IL-4/IL-10 transwell co-culture TAMs were the best representation of *in vivo* TAMs as they showed mixed TAM subpopulations, an increase in M2-like populations over the course of co-culture, and increased IL-10 secretion. Unfortunately, *in vitro* direct co-culture TAMs did not reflect the same complexity of subpopulations and M2-like properties as the transwell co-culture TAMs. However, IL-4/IL-10 cytokine treatment may improve this.

Conclusions and Future directions

The *in vitro* IL-4/IL-10 transwell co-culture TAM model best mimics *in vivo* TAMs with its mix of inflammatory (M1) and anti-inflammatory (M2) properties. Future directions include:

1. Treating *in vitro* direct co-culture TAMs with IL-4/IL-10 cytokines
2. Establishing *in vitro* and *in vivo* TAM models with murine colon adenocarcinoma MC38 tumour cells
3. Beginning VACV infection studies *in vitro* using the IL-4/IL-10 transwell co-culture TAM model

Acknowledgements

We thank members of the Cassol lab, Turnstone Biologics, the Mitacs Accelerate program, and NSERC for their research support and/or financial aid.

References

1. Lecoultre M, Dutoit V, Walker PR. Phagocytic function of tumor-associated macrophages as a key determinant of tumor progression control: a review. J Immunother Cancer. 2020 Dec;8(2).

2. Cao F, Nguyen P, Hong B, DeRenzo C, Rainusso NC, Rodriguez Cruz T, et al. Engineering Oncolytic Vaccinia Virus to redirect Macrophages to Tumor Cells. Adv Cell Gene Ther. 2021 Apr;4(2).

1st TEAM Hub Workshop
Ottawa, ON
June 26-28, 2023

TEAM Hub
Tissue Engineering & Applied Materials

Developing 3D tumor model using bioprinting technology for evaluating the effect oncolytic virus (OV) therapy on tumour associated macrophages (TAMs)

A. Fareghdeli[1,2], R. Skilling[2], D. Ahmed[2], Z. Versey[2], E. Cassol[2] and L. Leila Mostaço-Guidolin[1]

[1]Department of Systems and Computer Engineering, Carleton University, Ottawa, Canada
[2]Department of Health Sciences, Carleton University, Ottawa, Canada

Introduction

Tumor microenvironment (TME) is a dynamic, heterogenous, and complex environment consisting of different types of cells and biomolecules [1]. Specific physio-chemical characteristics of TME, such as extracellular matrix (ECM) components, pH, and oxygen concentration affect on tumor-immune system interaction, which further play a key role on tumor invasion, metastasis, and drug efficacy [2][3]. Providing 3D culture models with customized microenvironment facilitates evaluating tumor-immune cells crosstalk while maintaining complexity of the TME [1]. Bioprinting is an emerging technology which enables researchers to develop precisely controlled 3D tumor models [4]. These models can be employed to assess oncolytic virus (OV) therapy *in-vitro* in which viruses infect the tumor cells and while trying to copy themselves, destroy the tumor cells by bursting them and activate the immune system [5]. The aim of this work is to develop 3D *in vitro* models to evaluate the effect of OV on tumor associated macrophages (TAMs) within the TME.

Methodology

To develop 3D *in vitro* tumor models we must: i) ensure that all the required biomaterials are biocompatible; ii) adjust design parameters to emulate the biophysical, chemical and mechanical properties of TME *in vivo*; iii) define strategies to evaluate physio-chemical changes in TME on ECM composition and tumor-TAMs crosstalk.

For this end, cell viability will be investigated by MTT assay and confocal microscopy. The ECM composition and cellular morphology in TME will be analysed by Second harmonic generation (SHG) microscopy. Moreover, the production of cytokine and gene expression in tumor models will be assessed by ELISA, flow cytometry, and RT-PCR. Tumor models' mechanical properties will be examined by atomic force microscopy (AFM).

The first step in this work has been evaluation of alginate cytotoxicity which was assessed by methylthiazolyldiphenyl-tetrazolium bromide (MTT) assay using RAW 264.7 cells. In this experiment, the effect of five alginate concentrations and three cell concentrations on cell viability was evaluated.

Preliminary And Expected Results

Since alginate is a Food and Drug Administration (FDA) approved hydrogel, it was expected to be biocompatible. Preliminary results from the MTT assay in Figure 1 confirmed their biocompatibility. Even though no trend was observed in the cell viability, it indicated a relationship between alginate and cell concentration with the metabolic activity of the cells that might be related to cell proliferation. Moreover, statistical analysis confirmed the significant effect of cell and alginate concentration on cell viability ($p<0.05$). Although more than 90% cell viability was observed, additional assessment of activation status will be performed.

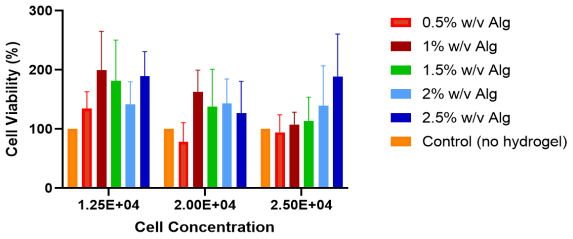

Fig. 1. Evaluating the effect of cell and alginate concentration on cell viability with the MTT assay.

Conclusions

Bioprinting technology shows great promise in developing 3D cancer models to recreate the complex TME which is very favorable to evaluate immune–tumor cells crosstalk in antitumor applications. So far, cell viability assay demonstrated the cytocompatibility of alginate hydrogel as a potential bioink for developing tumor models. But further analysis is required to develop bioinks compatible with tumor mechanical and biochemical environment traits.

Acknowledgements

This work is funded and supported by Mitacs Accelerate program and Turnstone Biologics.

References

1. Y. Kang, *ACS Applied Bio Materials*, 2020.
2. L. M. Sencha, *Int J Mol Sci*, 2022.
3. C. Vitale, *Cancers (Basel)*, 2022.
4. R. Staros, *Cancers*, 2022.
5. M. Keshavarz, *International Immunopharmacology*, 2022.

1st TEAM Hub Workshop
Ottawa, ON
June 26-28, 2023

TEAM Hub
Tissue Engineering & Applied Materials

Effect of BRCA Mutation and Metformin use on Premature Ovarian Aging

A. Murray[1,2], D. Landry[3], C.W. McCloskey[1,2], D. Trudel[4], A.M. Mes-Masson[4], R. Drapkin[5] and B.C. Vanderhyden[1,2]

[1]University of Ottawa/Cellular and Molecular Medicine, Ottawa, Canada
[2]OHRI/Cancer Therapeutics Program, Ottawa, Canada
[3]University of Ottawa/Health Sciences, Ottawa, Canada
[4]Centre de recherche du Centre hospitalier de l'Université de Montréal/Institut du cancer de Montréal, Montreal, Canada
[5]University of Pennsylvania/School of Medicine, Philadelphia, United States of America

Introduction

Ovarian cancer is the 5th leading cause of cancer-related mortality for women in Canada, with a poor 5-year survival rate of 44% [1]. Effective screening for early detection of ovarian cancer unfortunately does not exist and treatment options are limited for higher staged cancers [2]. Individuals who carry a germline mutation in *BRCA1/2* genes (which are involved in DNA repair) are at a higher risk of developing ovarian cancer [2]. Risk reduction among mutation carriers, involves radical interventions such as surgical removal of both ovaries and fallopian tubes or use of oral contraceptives [2, 3]. Age and total number of life-time ovulations are primary risk factors for the development of ovarian cancer. We have previously shown that ovarian fibrosis (defined as increased collagen deposition and linearization) develops in an age-dependent manner and is present in human post-menopausal ovaries but is usually absent in pre-menopausal ovaries [3]. We have also shown that in mice, treatment with metformin, a drug commonly used to control and treat Type 2 Diabetes Mellitus (T2DM) prevents age-associated ovarian fibrosis by changing the proportion of fibroblasts, myofibroblasts and immune cells found within the ovarian microenvironment [4]. The current study aims to gain further understanding of the preventative effect of metformin on ovarian aging and fibrosis in the human population, specifically *BRCA1/2* mutation carriers.

Methodology

We aim to achieve this through the investigation of a cohort of 100 human ovary samples collected from Centre de recherche du Centre Hospitalier de l'Université de Montréal (CRCHUM) and The OCRC Tumor BioTrust Collection in Philadelphia, PA. This cohort includes samples from both pre- and post-menopausal *BRCA1/2* mutation carriers and non-carriers, as well as from patients who had been treated with metformin pre-oophorectomy. Ovaries have been sectioned, formalin-fixed and paraffin embedded (FFPE) for subsequent staining and genetic analysis. Picrosirius red stain was used to look for the presence of collagen fibers within the ovarian stroma. Next, we plan on performing microdissection of the ovarian cortex from all human ovary samples using the AVENIO Millisect System (Roche), which will be followed by RNA isolation using the RNeasy FFPE Kit (Qiagen). RNA quality will be assessed using a Fragment Analyzer (Agilent) and RNA concentration with a NanoDrop One Spectrophotometer (Thermo-Scientific). Samples will then be sent for transcriptomic analysis to assess differential expression of fibrosis- and immune-associated genes using NanoString arrays.

Results

We have preliminary data that shows that natural ovarian aging is accompanied by the development of age-associated ovarian fibrosis that becomes evident during or after the onset of menopause in non-carriers, whereas *BRCA* mutation carriers tend to develop fibrosis earlier, at pre-menopausal ages.

Table 1. Preliminary fibrosis data in human ovary samples pre- and post-menopausal stratified by *BRCA* status

Menopausal Status	*BRCA* Status/Other Risk Factors (RFs)	Total fibrotic ovaries
Pre-menopausal	WT (Wild Type *BRCA*)	1/3 (33%)
	WT with non-*BRCA* RFs	2/3 (66%)
	BRCA1/2+	3/5 (60%)
Post-menopausal	WT	5/6 (83%)
	BRCA1/2+	6/7 (86%)

Conclusions

The aim of this study is to further elucidate the relationship between ovarian aging and fibrosis that has previously been established by the Vanderhyden lab. With this large cohort of human ovary samples, we hope to uncover the processes that promote the early onset of ovarian fibrosis within *BRCA* mutation carriers, in addition to investigating the effects of metformin as a prophylactic treatment for ovarian fibrosis in women at high risk for the development of ovarian cancer, such as *BRCA* mutation carriers.

Acknowledgements

We would like to honour and acknowledge the late Margaret Craig whose generous support has funded the majority of this study. This project has also received funding from a grant from the Canadian Institutes of Health Research (E-436754).

References

1. Canadian Cancer Society, "Cancer Specific Stats-2022", 2022.
2. U. Matulonis *et al*, "Ovarian Cancer," NRDP, vol. 2, 16061, 2016.
3. C. W. McCloskey *et al*, "Metformin Abrogates Age-Associated Ovarian Fibrosis," Clin Cancer Res, vol. 26(3), pp. 632-642, 2020.
4. D. Landry, *et al*, "Metformin prevents age-associated ovarian fibrosis by modulating the immune landscape in female mice," Sci Adv, vol. 8, eabq1475, 2022.

1st TEAM Hub Workshop
Ottawa, ON
June 26-28, 2023

TEAM Hub
Tissue Engineering & Applied Materials

Investigating the Relationship between BRCA Mutations and Ovarian Cancer

O.R. Piccolo[1,2], H.T. Vaishnav[1,2] and B.C. Vanderhyden[1,2]

[1]Department of Cellular and Molecular Medicine, University of Ottawa, Ottawa ON, Canada
[2]Cancer Therapeutic Program, Ottawa Hospital Research Institute, Ottawa ON, Canada

Introduction

Ovarian cancer is the most lethal gynecological malignancy and the 5th leading cause of cancer-related deaths in women worldwide (1). Age and total lifetime ovulations are primary non-hereditary risk factors for ovarian cancer. Due to repeated extracellular matrix (ECM) remodeling and inflammation that occurs with each ovulation, it is possible that over time, tissue homeostasis is disrupted. Eventually, this may lead to age-associated ovarian fibrosis, which is the excessive deposition of anisotropic collagen fibers and is thought to be a risk factor for cancer (2). Though the cause of age-associated ovarian fibrosis is currently unknown, it is possible that changes in ovarian cells, specifically fibroblasts, may be a driving factor for the development of fibrosis and specifically the accumulation of senescent myofibroblasts (3). Using single-cell RNA sequencing, we identified a population of senescence-associated secretory phenotype (SASP) producing fibroblasts unique to the aged murine ovary (4).

In preliminary studies in our lab, we identified that *BRCA1*/2 mutation carriers, a population at higher risk for ovarian cancer, have ovaries that develop fibrosis at pre-menopausal ages, whereas this was evident mostly at post-menopausal ages for non-carriers (Table 1). These findings, in combination with the fact that the median age of onset for ovarian cancer in *BRCA1* mutation carriers is almost two decades earlier than non-carriers, suggest an association between ovarian fibrosis and cancer. While the mechanisms underlying the accelerated onset of ovarian fibrosis in mutation carriers remain to be elucidated, evidence suggests that loss of *Brca1* in primary murine ovarian fibroblasts (MOFs) *in vitro*, renders them senescent and induces myofibroblast activation. We hypothesize that *Brca1* loss in ovarian fibroblasts facilitates their transition into senescent cells, accelerating the onset of ovarian fibrosis and consequently posing an increased risk for ovarian cancer.

Methodology

As fibroblasts are the primary cell type responsible for ECM remodeling, we isolated and optimized culture conditions for MOFs from mice with *Brca1* floxed with loxP. MOFs were transduced with adenovirus expressing cre recombinase to create *Brca1* knockout (KO) MOFs, and were compared to the wild-type by RNA sequencing. To determine the effects of *Brca1* KO *in vivo*, FoxD1-Cre-ER^{T2} mice will be bred with *Brca1*-loxP/loxP mice to create FoxD1-Cre-ERT2; *Brca1*-loxP/loxP mice. FoxD1 is a promoter specific to fibroblasts and pericytes. FoxD1 activation, through tamoxifen administration, drives Cre-ER^{T2} protein expression. Intrabursal injection of tamoxifen to the ovary would create ovarian fibroblast-specific *Brca1* KO. Ovaries will be collected at different time points and assessed for fibrosis using Picro Sirius Red to visualize collagen.

Results

The Vanderhyden lab has previously revealed a subset of fibroblasts in the aged mouse ovary characterized by SASP expression (SASP fibroblasts-Fig. 1). Further, in support of our hypothesis, preliminary data from RNA sequencing of *Brca1* KO MOFs revealed a gene expression profile similar to myofibroblasts, suggesting that the accumulation of senescent myofibroblasts in the ovary may be responsible for the onset of fibrosis observed in *BRCA* mutation carriers.

Table 1 - Unpublished data from C. McCloskey describing pre-menopausal *BRCA* mutation carriers or non-carriers and presence of ovarian fibrosis.

Group	Age	*BRCA* status	Total fibrotic ovaries
Pre-menopausal	32-45	wt	3/10 (30%)
	35-45	*BRCA*+	3/5 (60%)
Post-menopausal	61-82	wt	5/6 (83%)

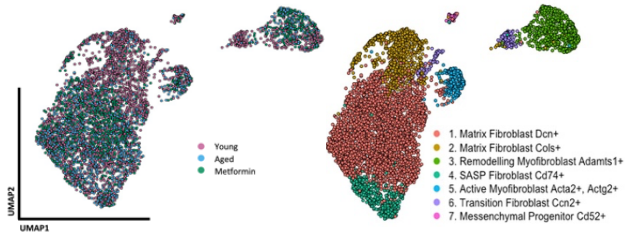

Fig 1. Changes in the population of cells in young, aged, or metformin-treated mice from Landry et. al. 2022.

Conclusions

This study will provide insight into the association between *Brca1* mutations and ovarian cancer risk, and lay the groundwork for future investigations into prophylactic drugs to delay or prevent the onset of ovarian fibrosis.

Acknowledgements

We acknowledge the late Margaret Craig, whose generous contribution funded much of this study. This study will also be funded by a Canadian Institutes of Health Research grant.

References

1. McCloskey, Curtis W., et al. "Metformin Abrogates Age-Associated Ovarian Fibrosis." *Clinical Cancer Research*, vol. 26, no. 3, 2020, pp. 632–642, https://doi.org/10.1158/1078-0432.ccr-19-0603.
2. Landry, David A., et al. "The Significance of Ovarian Fibrosis." *Oncotarget*, vol. 11, no. 47, 2020, pp. 4366–4370, https://doi.org/10.18632/oncotarget.27822.
3. Hinz, Boris, and David Lagares. "Evasion of Apoptosis by Myofibroblasts: A Hallmark of Fibrotic Diseases." *Nature Reviews Rheumatology*, vol. 16, no. 1, 2019, pp. 11–31, https://doi.org/10.1038/s41584-019-0324-5.
4. Landry, David A., Edward Yakubovich, et al. "Metformin Prevents Age-Associated Ovarian Fibrosis by Modulating the Immune Landscape in Female Mice." *Science Advances*, vol. 8, no. 35, 2022, https://doi.org/10.1126/sciadv.abq1475.

1st TEAM Hub Workshop
Ottawa, ON
June 26-28, 2023

TEAM Hub
Tissue Engineering & Applied Materials

Stimulated Raman scattering microscopy to investigate radiation stress response in MCF7 cancer cells

C.H. Allen[1,2], J.R. Gagnon[1], R. Skillings[3], D. Ahmed[3], S.C. Sanchez[4], K. Altwasser[4], G. Hilan[5], W.G. Willmore[5], V. Chauhan[4], E. Cassol[3], and S. Murugkar[1,2]

[1]Carleton University, Department of Physics, Ottawa, Canada
[2]Carleton University, Ottawa-Carleton Institute for Biomedical Engineering, Ottawa, Canada
[3]Carleton University, Department of Health Sciences, Ottawa, Canada
[4]Health Canada, Consumer and Clinical Radiation Protection Bureau, Ottawa, Canada
[5]Carleton University, Institute of Biochemistry, Department of Biology and Chemistry, Ottawa, Canada

Introduction

Altered lipid metabolism of cancer cells has been implicated in increased radiation resistance. A better understanding of this phenomenon may lead to improved radiation treatment planning. Current techniques based on fluorophore probes to visualize intra-cellular lipids risk altering the inherent biophysical properties of the lipids. Here we demonstrate a label-free technique based on stimulated Raman scattering (SRS) microscopy to investigate the radiobiological response in human breast cancer MCF7 cells, focusing on how ionizing radiation exposure affects lipid droplet (LD) distribution and cellular morphology.

Methodology

Raman spectroscopy involves the inelastic scattering of light due to vibrations of chemical bonds. It is a label-free method that provides biochemical signatures of multiple macromolecules in a single acquisition. However, since the spontaneous Raman signal is very weak, long acquisition times are needed for imaging cell and tissue samples. In contrast, SRS microscopy is a coherent Raman imaging technique that offers more than 1000-times faster imaging speed with sub-cellular resolution and intrinsic 3D sectioning, making it much more practical for high spatial resolution imaging.

Here, we use a custom-built SRS microscopy setup (Fig. 1) to collect SRS images of MCF7 breast cancer cells exposed to either 0 or 30 Gy (X-ray) ionizing radiation every 24 hours over a period of 72 hours [1]. SRS images were analyzed to quantify changes in lipid droplet area per cell, and lipid and protein content per cell.

Results

To determine the changes in lipid metabolism, we imaged both unirradiated (Fig. 2a,b) and irradiated (Fig. 2c,d) MCF7 cells at the 2850 cm^{-1} (CH_2) band with contributions predominantly from lipids, and at the 2926 cm^{-1} (CH_2, CH_3) band with overlapping contributions from proteins and lipids. Lipid-rich and protein-rich images were then obtained for lipid and protein content analysis by applying multivariate curve resolution alternate least-squares, and a threshold mask was then applied to determine lipid droplet area.

Total lipid and protein intensities per cell showed significant increases after 48 and 72 hours in the 30 Gy cells compared to the control. LD area per cell was also found to increase with time, with greater mean LD area per cell for irradiated than control.

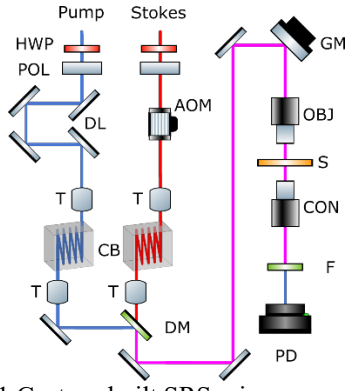

Fig. 1 Custom-built SRS microscopy setup

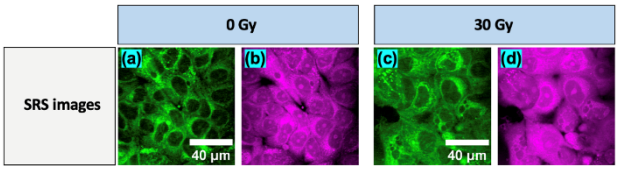

Fig. 2 Representative SRS images of MCF7 cells at 2850 cm^{-1} (green) and 2926 cm^{-1} (magenta) for unirradiated (a,b) and irradiated (c,d) cells.

Conclusions

This pilot study demonstrates the potential of SRS imaging for investigating ionizing radiation-induced changes in cancer cells without fluorescent labels.

Acknowledgements

This research was supported by the NSERC Discovery Grant (S.M., E.C., and W.G.W.).

References

1. C.H. Allen et al., "Investigating ionizing radiation-induced changes in breast cancer cells using stimulated Raman scattering microscopy" under review (2023).

1st TEAM Hub Workshop
Ottawa, ON
June 26-28, 2023

TEAM Hub
Tissue Engineering & Applied Materials

Towards the development of Raman Spectroscopy for blood-based biodosimetry

A. Beausoleil-Morrison[1], C. McNairn[1], X. Qin[2], C. Ciobanu[3], K. Altwasser[4], S. Subedi[2], V. Chauhan[4] and S. Murugkar[1]

[1] Department of Physics, Carleton University, Ottawa, Canada
[2]Department of Mathematics and Statistics, Carleton University, Ottawa, Canada
[3]Department of Physics, McGill University, Montreal, Canada
[4]Health Canada, Ottawa, Canada

Introduction

Biodosimetry is key technique for emergency management following unplanned exposures to ionizing radiation. Current biodosimetry techniques are time-consuming and labour-intensive. Raman spectroscopy of blood is a light-based, non-invasive and label-free technique that has been shown by our team to have promising potential for biodosimetry [1]. In this follow-up pilot study we investigated the application of Raman spectroscopy and multivariate analysis for biodosimetry based on blood plasma [2].

Methodology

Blood from a single donor was irradiated with X-rays at three doses: 0 (control), 5 and 20 Gy. Blood plasma was divided equally into 18 aliquots and frozen. Raman spectra of the blood plasma were acquired with a custom-built Raman microscope (Fig.1). Six technical replicates were obtained on different days (batches), consisting of a sample of each dose. Standard spectral preprocessing techniques for noise reduction and standardization were applied to these data. The dose separation was analyzed using Partial Least Squares Discriminant Analysis (PLS-DA). Sparse PLS-DA (sPLS-DA) was used to improve the dose separation by filtering out Raman bands not associated with dose separation in the model. A batch-effect correction algorithm involving a random-effects model was applied to account for variance between replicates.

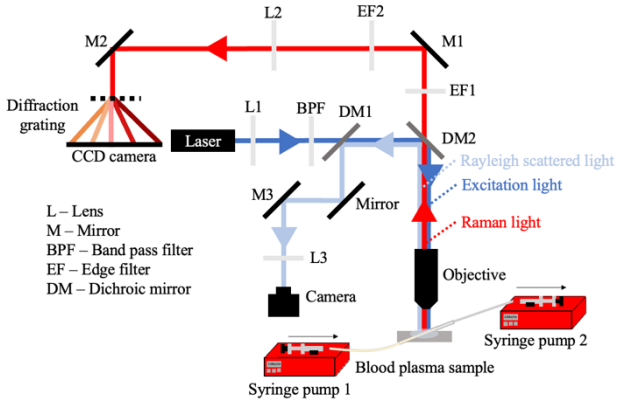

Fig.1: Schematic of Benchtop Raman Microscope

Results

Although PLS-DA scores plots showed dose separation in each individual batch, clear dose separation was not evident when applying this technique to the data from different batches. In contrast, after correcting for this batch effect, and utilizing sPLS-DA, the dose overlap and clustering effects were significantly reduced (Fig.2). Loadings vectors from sPLS-DA highlighted regions in the Raman spectra related to the observed separation between doses corresponding to potentially radiation-sensitive biomarkers.

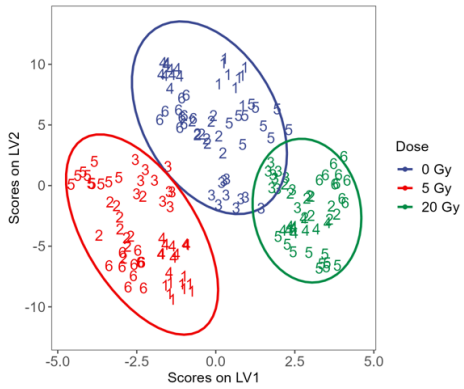

Fig. 2: Sparse PLS-DA scores showing dose separation for Raman spectra of blood plasma after batch-effect correction.

Conclusions

Raman spectroscopy combined with multivariate analysis offers promising potential for blood-based biodosimetry.. Ongoing work involves expanding this study to include multiple donors.

Acknowledgements

NSERC Discovery Grant (S.M. and S.S.) and Carleton U.

References

1. Ciobanu, C. et al, Radiat Res. 199(4):396-405 (2023).
2. Beausoleil-Morrison, A., McNairn, C., et al, Proc. SPIE 12373, (2023).

1st TEAM Hub Workshop
Ottawa, ON
June 26-28, 2023

Development of in vitro airway models for asthma

"N. Abzan[1]", "W. Willmore[2]", "L. Mostaco-Guidolin[3]"

[1] Carleton University/Systems and Computer, Ph.D. student, Ottawa, Canada
[2] Carleton University/Biology, Professor, Ottawa, Canada
[3]Carleton University/System and Computer, Assistant Professor, Ottawa, Canada

Introduction

Asthma is a chronic lung disease. The symptoms of asthma include wheezing, coughing, a tight chest, and breathlessness [1]. According to the Global Asthma Report, the number of asthmatic patients will increase to 400 million worldwide by 2025 [2]. In asthma, in a process called 'airway remodeling', the structure and composition of the airways change, which leads to a thickened airway wall, also known as fibrosis [4]. In airway fibrosis, the excess production of collagen, the most abundant protein in the lung extracellular matrix (ECM), results in airway narrowing and eventually breathing difficulties. Moreover, the accumulation of collagen changes the structure and composition of the lung ECM. This affects the functions of ECM in providing vital biomechanical and biochemical cues to regulate cellular responses [1]. Key fundamental processes associated with fibrosis are not entirely understood. Moreover, the interactions between the ECM and tissue-resident cells as well as the mechanisms that drive ECM remodeling (reorganization of existing tissue) remain unclear [3]. In this work, we are developing an air–liquid interface (ALI) multi-layered *in vitro* model of lung airways using a novel microfluidics-based 3D bioprinter and other approaches.

Methodology

In order to investigate the mechanisms driving fibroblasts in airway remodeling, we will establish cell culture systems of primary lung fibroblasts (WI-38) and epithelial cells (A549). The experimental steps include establishing: i) a 2D single culture of fibroblasts, ii) ALI 2.5D co-culture of both fibroblasts and epithelial cells, and iii) a 3D hollow-tube model with both cell types, as shown in Fig.1. Each of these models will be exposed to hypoxia (low oxygen condition) and we will assess the cellular responses via several assays including western blot and gene expression. The models will also be characterized using nonlinear optical microscopy (NLOM) to resolve the biochemical and 3D structural composition of airway ECM components, more specifically collagen. Moreover, Raman micro-spectroscopy will resolve complex cell phenotypes and the structural composition of ECM proteins. The 3D bioprintability and cell viability of the collagen-based bio-ink formulation will be investigated.

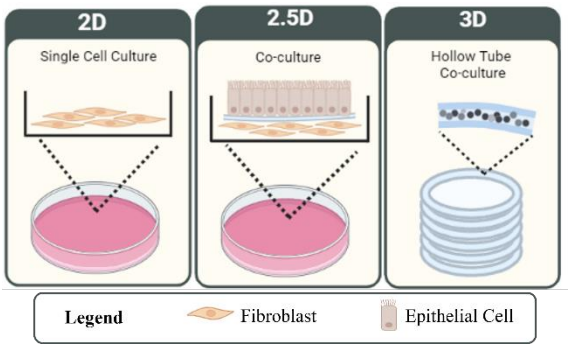

Fig.1. Cell culture systems of lung fibroblasts and epithelial cells envisioned to assess the effects of hypoxia on collagen remodelling: i) 2D single culture of fibroblasts, ii) ALI 2.5D co-culture of both fibroblasts and epithelial cells, and iii) a 3D dynamic hollow-tube model with both cell type.

Expected Results

The co-culture model of fibroblasts and epithelial cells will allow for cellular communication through the release of soluble factors, which will mimic *in vivo* conditions in the airways. Investigating the effects of hypoxia on collagen/ECM remodeling in an ALI model is crucial to reveal how changes in oxygen concentration can affect the biosynthesis process of collagen by fibroblasts, leading to ECM structure alternations in asthma. 3D bioprinted models allow for understanding the dynamic changes of the ECM protein profile during asthma development and progression.

Conclusions

The combination of 3D *in vitro* models, complex cell cultures, and imaging methods in the current research will determine the basic mechanisms of cell-ECM interactions as well as understand the role of oxygen in lung ECM formation and remodeling in asthmatic patients. This work will serve as a stepping stone toward the development of novel therapeutic strategies for asthma and other chronic respiratory diseases.

Acknowledgements

This work is supported by NRC Ideation Fund (2020-177), NSERC-DG (RGPIN-2021-04185), and WW (RGPIN-2017-06414).

References

[1] J. K. Burgess et al., *European Respiratory Review*, 2022.
[2] J. T. Ito, et al., *Cells,* 2019.
[3] Y. Bossé et.al., *Curr Allergy Asthma Rep*, 2008.

1st TEAM Hub Workshop
Ottawa, ON
June 26-28, 2023

TEAM Hub
Tissue Engineering & Applied Materials

Mapping Airway Remodeling in Asthma using Multimodal Raman-Second Harmonic Generation Imaging and Machine Learning

N.N. Kunchur, Leila Mostaco-Guidolin
Carleton University, Department of Systems and Computer Engineering, Ottawa, Canada

Introduction

Asthma is a chronic inflammatory airway disease, which leads to structural changes, broadly referred to as airway remodeling [1]. Inhaled aeroallergens, viruses and pollution inflict tears on the epithelial barrier lining the airways, inducing an inflammatory fibrotic response to remodel the damaged tissue [2]. Subepithelial fibrosis (SF) is one of the major hallmarks in the pathology of asthma and is denoted by the excessive accumulation of extracellular matrix (ECM) proteins; particularly collagen I [3]. Evidence suggests it leads to tissue stiffening and a reduction in lung function [4]. Traditional methods used to visualize changes in asthmatic lung tissue (i.e. histology) lack specificity in detailing the biochemical and structural information of ECM proteins being deposited within asthmatic airways [5]. Leveraging the technologies of both Raman microspectroscopy (RM) and second harmonic generation (SHG), a novel label-free multimodal imaging system (multimodal RM-SHG) allows for the high-resolution visualization of ECM proteins contributing to airway remodeling. Due to the complex nature of the data obtained, the development of novel approaches based on machine learning (ML) strategies to identify biomarkers associated with airway remodeling in asthma is necessitated. In this work, we aim to:

i. Evaluate the distribution of definitive biomolecules in asthmatic and non-asthmatic control airways;
ii. Develop machine learning-based strategies to isolate key biochemical signatures of differing airway regions;
iii. Create an open-source library with airways/lung tissue biochemical signatures;
iv. Identify novel biomarkers associated with asthmatic airway remodeling.

Methodology

Airway lung tissue of ten asthmatic and ten non-asthmatic subjects not suitable for transplantation are obtained through our established collaboration with UBC-heart lung innovation. Frozen lung tissue sections of individuals from both sexes and different ages are used, including cases of fatal asthma. Using multimodal RM-SHG, each pixel in the imaged tissue contains a biochemical signature unique to that specific location. RM-SHG outputs the spatial biochemical maps of tissues and cells with 300 nm spatial resolution without disrupting tissues with exogenous stains, as shown in Figure 1. For the first time, the structural and biochemical profiles of the epithelium, basement membrane, and lamina propria of airways will be obtained through Raman, with the fibrillar collagen deposition simultaneously imaged using SHG. Supervised machine learning and deep learning-based strategies (including multilayer perceptron networks and convolutional neural networks) will assess the spectra-based images and curate an open-source library of spectral signatures associated with biomolecules specific to lung/airways tissue (e.g. protein-specific bands). Collagen abundance and the roles of ECM-specific biomolecules in airway remodeling of the epithelium, basement membrane, and lamina propria will be identified using developed ML automated classification pipeline.

Results

Using RM, preliminary analysis denotes spectral differences between the epithelial, basement membrane and lamina propria tissue layers of airways as shown in Figure 1. Contrary to our current understanding of the SF pathway, there is an unexpected absence of fibrillar collagen I in the basement membrane when imaged using SHG. These findings challenge SF being a response from fibroblasts synthesizing collagen I in its fibrillar form to remodel damaged tissue. With the ongoing development of an automated classification pipeline leveraging both supervised machine learning (ML) and deep learning, the imaged spatial biochemical maps will be used to train models capable of denoting the exact spectral differences amongst healthy and asthmatic lung tissue. RM signatures will be traced to match protein-specific spectral bands unique to diseased asthmatic lung tissue. With the aid of ML, multimodal RM-SHG images will guide the curation of an open-source library of spectral signatures of biomolecules and proteins present in asthmatic lung tissue.

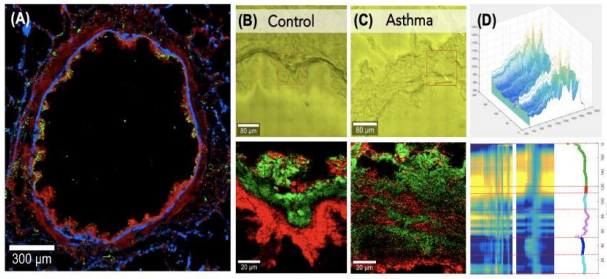

Figure 1. Representative images showing biochemical spatial maps of a whole (A) airway (red: lipids; blue: proteins; green: surfactants). Examples of (B) control and (C) asthmatic airways biochemical maps showing detailed distribution of proteins (green, collagen) and lipids (red, C-H bonds). (D) Each pixel of the images are associated to a spectrum, which provides information about the biochemical composition of each location, able to capture changes with a spatial resolution of 300 nm, and track the composition of different tissue layers.

Conclusions

This research is the first to integrate two novel technologies, multimodal RM-SHG and ML to investigate ECM-specific biochemical signatures of different tissue layers. Insight into the fibrotic responses in asthma with an unprecedented level of spatial and biochemical specificity will drive the identification of biomarkers active in airway remodelling. This work holds the potential to direct new avenues in developing therapies aimed at preventing and minimizing the formation of scar tissue observed through the excessive burden of SF.

References

1. J. W. R. B. S. H. WilliamR. Roche, "Subepithelial Fibrosis in the Bronchi of Asthmatics," *The Lancet,* vol. 333, no. 8637, pp. 520- 524, 1989.
2. S. M. P. S. F. J. H. V. B.-H. I. P. H. M. H. E. V.-W. D. S. N. B. C. C. J. S. R. D. P. H. H. J. E. C. Chang Xiao, "Defective epithelial barrier function in asthma," *Journal of Allergy and Clinical Immunology,* vol. 128, no. 3, pp. 549- 556, 2011.
3. T. A. Wynn, "Cellular and Molecular Mechanisms of Fibrosis," *The Journal of Pathology,* vol. 214, no. 2, pp. 199-210, 2008.
4. M. L. C. T. J. B. R.-M. L. J. T. J. S. D. V. J. T. Kenneth P. Hough, "Airway remodeling in asthma," *Front Med (Lausanne),* vol. 191, no. 7, 2020.
5. T. A. Wynn, "Cellular and Molecular Mechanisms of Fibrosis," *The Journal of Pathology,* vol. 214, no. 2, pp. 199-210, 2008.

1st TEAM Hub Workshop
Ottawa, ON
June 26-28, 2023

TEAM Hub
Tissue Engineering & Applied Materials

Evaluation of the effect of sample preparation in collagen fibres via Second Harmonic Generation Imaging

A. Kaianathbhatta[1] , D. Ahmed[2], R. Skillings[2], Z. Versey[2], E. Cassol[2] and L. Mostaço-Guidolin[1]

[1] Carleton University/Department of Systems and Computer Engineering, Ottawa, Canada
[2] Carleton University/Department of Health Sciences, Ottawa, Canada
MASc. Biomedical Engineering

Introduction

To study diseases, we rely on different samples, which must first be prepared before assessment. Sample preparation includes different steps including - but not limited to freezing, staining, and sectioning. The main question this research aims to answer is to what extent tissue collagen changes when different types of sample preparations are conducted. Changes in collagen structure are often a hallmark of different pathological conditions and this study will involve three major components: evaluation of the effect of sample preparation on *ex vivo* tissues, and 3D bioprinted tissues as well as imaging and image processing. These three components will be investigated and will play a crucial role in answering this fundamental but important question.

Methodology

Tissues from mice were harvested. Trachea, liver and heart tissue samples are being imaged, following the 5 sample processing protocols: fresh tissue, frozen tissue placed in a -80 freezer, frozen in a -80 freezer after the snap freeze, frozen in a -80 freezer after embedding tissue in 10% DMSO+PBS solution, and fixed samples using a 1:10 formalin solution. The tissue preparation has been done on bulk tissue sections, and in the future all tissues will be sectioned, processed and imaged as well.

Samples were imaged using a Zeiss LSM 980 confocal microscope with multiphoton capability. A femtosecond laser centred at 800 nm was used. Images were acquired with a scan speed of 4µs, and 2 to 4x averages were applied in order to increase the signal-to-noise ratio (SNR), and a 63x/ 1.4 oil plan-apochromat objective was used.

An image processing pipeline will be implemented to first filter out noise in the images, and then textural features will be extracted to quantify the changes the sample preparation does to the collagen. All of the image processing will be performed in Python, with pre-processing performed on Zeiss lite image processing and Fiji.

The next steps are be to perform sample preparation and imaging of 3D bioprinted tissues. In addition, collagen structural changes will be classified and quantified by extracting textural features. This classification will be included in the image processing pipeline, which will enhance, filter and extract textural features to quantify the changes.

Preliminary Results

Figure 1a shows the clear fibrillar collagen structure. The fixed sample shows some structure but overall is not as organized and structured as the fresh tissue image. These preliminary images are the first steps toward gaining useful insight into the structural changes of collagen due to sample processing.

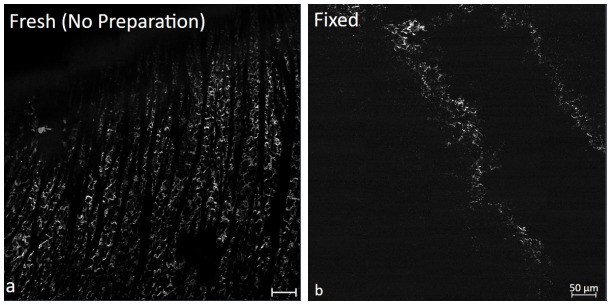

Fig. 1 . Fresh lung SHG images using the Zeiss LSM 980 x63 Oil immersion lens. a) Collagen fibres at an emission of 393nm, and excitation of 800nm. The image was converted to grayscale on Zen lite. b) Fixed lung sample after an excitation of 900nm, emission at 449nm. The image was converted to grayscale on Zen lite.

Conclusions

This study focuses on how collagen structure in the liver, trachea, and heart changes in *ex vivo* tissues and in bioengineered tissues when frozen and fixed. By focusing on collagen fibrillar structure, SHG imaging is powerful as it is biochemically specific to non-centrosymmetric structures. Collagen type I has this structure, ensuring a second harmonic signal can be generated. Finally, understanding how to classify and quantify the changes is useful in determining the best tissue processing protocols for biomedical sample processing.

Acknowledgements

This work is supported by NSERC-DG (RGPIN-2021-04185) and the Cassol Lab in the Department of Health Sciences, Carleton University

References

1. Mostaço-Guidolin, L. et al. Int. J. Mol. Sci., 2017.
2. Poole, J. A. J, CU, MASc dissertation, 2022

1st TEAM Hub Workshop
Ottawa, ON
June 26-28, 2023

TEAM Hub
Tissue Engineering & Applied Materials

Mathematical models for mapping cellular dynamics on bioengineered in extracellular matrix

Contesini, G.S.[1], Leila, Mostaço-Guidolin[1]

[1] University of Carleton/Dep. of Systems and Computer Eng.Ottawa, Canada

Introduction

Fibrosis is a respiratory condition characterized by the increased deposition of collagen in tissues. In the lungs, it reduces the natural capacity to breathe, by affecting the tissue structure. And that, in all, accounts for half a million deaths yearly in the Americas alone [1,2]. This increase in collagen concentration is caused by myofibroblasts, a differentiated fibroblast cell, one of the key players during the wound healing process. Driven by the limited understanding of what triggers myofibroblasts to overproduce and remodel collagen, we are developing a mathematical model that describes, predicts, and informs the dynamics of cellular responses and tissue strain-stress deformations in the fibrotic tissues. More specifically, we investigate the interactions between MyoFibroblasts (MFs) and Extracellular Matrix (ECM), describing the relationship between ECM reshaping and stress straining of collagen fibers on MFs responses.

Methodology

In biology, there is a reduced number of invariant principles. Based on them, conservation laws can be asserted [4], and yet, within only a definite range, some conservation principles hold true [3]. Here, we consider the cellular density of a healthy MFs-ECM system (ρ) as constant. We impose Fick's first law of conservation (1), such that any time-variation in density is a consequence of a cell flux (J). Hence, all the dynamics of the system can be mapped as the contributions of cell confluence. This is known as the mechanical model for cellular dynamics [3,4], shown in Eq. (1):

$$\frac{\partial}{\partial t}\rho = -\nabla J \qquad (1)$$

Many biological mechanisms trigger cell growth and migration. Our mathematical study consists of a mechanical model for MFs-ECM interaction that focuses on the prime mechanisms that govern the transition from healthy normal density, to a fibrotic higher density ECM. Guided by experimental assessment, we consider the effects of Long and Short range Diffusion, Mechanotaxis, Chemotaxis, Contact Guidance and Inhibition, and Convection. We express these biological cues as mathematical terms, combining them into a differential equation. The solutions are obtained via well-established approximation methods and numerical simulations, such as, Poincaré–Lindstedt method, Green Function Solution, and Linearization.

Expected Results

Many factors influence the complex behavior of a cell. For example, the shape often hints on the possible role in its environment. In the case of MFs the filopodia, long-reach protrusions is an example of that figure (1). They allow MFs to sense tissue density far from its own local surroundings. Hence, we expected in short timescales, that this term dominates the overall behavior of the dynamics. On the other hand, If we analyze the system on a large timescale, we expect short range diffusion and cell mitosis terms to dominate the overall behavior. This discussion is an example of how rich and versatile analytical models can be. We relly and expect that a deeper analysis of our analytical model review insights of the different behaviors of MFs in ECM.

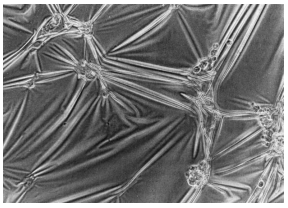

MFs on a silicon substrate. Filopodia can be observed reaching a neighbor four times the size of the cell. The shaded contrast shows the stress and deformation that these cells cause in the substrate. Image Source: [4].

Conclusions

From chemical, and mechanical cues, to tissue's density and shape, predicting the most crucial factors associated with fibrosis and tissue remodelling, allows us to better understand the complex dynamics in cellular micro environments. Although simple models are not a one-to-one representation of a real system, they are still powerful enough to provide valuable insights. As we increase the complexity of our mathematical models, we expect to better guide innovative *in-vitro* experiments, at a reduced cost and time with higher potential to impact our understanding of the fibrosis basic mechanisms.

References

1. Pan American Health Organization. https://www.paho.org/en/enlace/chronic-respiratory-disease-burden.
2. Canadian Pulmonary Fibrosis Fundation https://cpff.ca/understanding-pf/what-is-pulmonary-fibrosis/
3. May, R.M. doi:10.1126/science.1094442
4. Murray, J.D.,*et.al.* https://doi.org/10.1007/BF00277099
5. Murray, J.D. *ISBN-10: 0387952284* Vol. 3. New York: Springer, 2001.

The Microbiota of Pressure Injuries: Bacterial Dynamics and Antibiotic Tolerance in Polymicrobial Biofilm Infections

Allison K[1], Beaulieu C[1], Mejlaoui R[1], DeZeeuw K.G[2], Marek J.E[2], Latorre M[3], Mostaço-Guidolin L[3], Cassol E[1], Overhage J[1]

Department of Health Sciences[1], Carleton University, Ottawa ON, Canada
Department of Complex Continuing Care[2], Saint Vincent Hospital, Ottawa ON, Canada
Department of Systems and Computer Engineering[2], Carleton University, Ottawa ON, Canada

I. Introduction

In healthy individuals, wounds heal predictably via well-regulated biological processes. However, in elderly and immobile individuals, particularly those with predisposing co-morbidities, these processes can be dysregulated, resulting in the formation of non-healing chronic wounds [1]. Within these wounds, bacterial species can form robust and diverse multi-species biofilms to protect themselves from host immune responses and antibiotics [1]. Biofilms in chronic wounds typically consist of 2-10 different bacterial species [2]. Many single-species biofilm models typically studied in chronic wound research fail to account for the genetic and metabolic diversity of multiple microbial species found within chronic wound environments.

II. Methodology

With a focus on pressure injuries (PIs), this project utilizes common wound pathogens, e.g. *Staphylococcus aureus* (SA), *Pseudomonas aeruginosa* (PA), *Enterococcus faecalis* (EF), *Stenotrophomonas maltophilia* (SM), and *Escherichia coli* (EC) to develop an innovative in-vitro polymicrobial wound biofilm (PWB) model to study the role of biofilms in PIs. Biofilms were grown in Dulbecco's Modified Eagle Media in 12 well plates, harvested or imaged at different time points between 24-72 hours, and quantified using colony forming units (CFU) of each strain on selective agar plates.

III. Results

Using this PWB model, we are currently studying microbial community dynamics, interspecies interactions, and antibiotic tolerance of polymicrobial biofilms in order to better understand their contributions to the chronic wound environment. Initial results indicate that PA is a key pathogen in polymicrobial communities of PIs modulating species diversity within mixed biofilms by inhibiting the growth of certain species, while encouraging the growth of others (Fig 1).

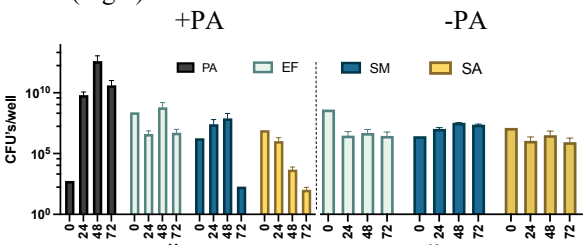

Figure 1: CFU counts of biofilms grown over 72 hours with and without PA.

Confocal laser scanning microscopy visualizes the biofilm dynamics and spatial organization of Gram-positive (EF, SA, red/orange) and Gram-negative (PA, SM, green) in biofilms grown for 24-hours. This model will allow us to visualize biofilm formation and species distribution over time (Fig 2).

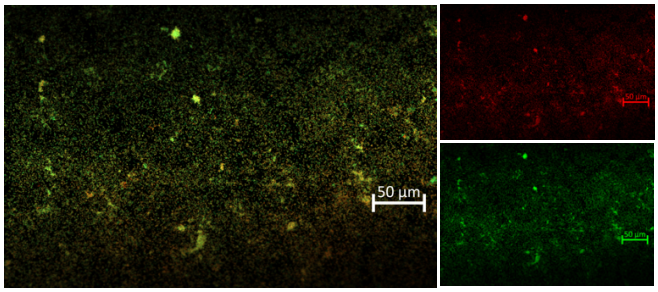

Figure 2: Fig 2: 24-hour PWB biofilms taken with ZEISS LSM 980 20x

We are analysing antibiotic susceptibility of single- and polymicrobial biofilms using our PWB model in combination with clinically relevant antibiotics, e.g., Ciprofloxacin (CIP). Initial results highlight how bacterial susceptibility in polymicrobial biofilms differs significantly compared to single-species biofilms, illustrating the recalcitrance of polymicrobial biofilm communities (Fig 3).

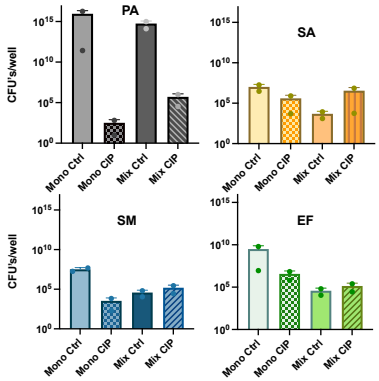

Figure 3: Cell counts of mono and mixed biofilms with and without 4 µg/mL CIP treatment (n=2).

IV. Conclusions

This research provides a model to study the fundamentals of how interspecies interactions affect biofilm formation, pathogenesis and antimicrobial resistance observed in PIs. Understanding these dynamics will progress chronic wound investigations to improve patient outcomes.

V. Acknowledgments

Special thanks to the physicians and nursing staff at Saint Vincent Hospital and to members of TEAM Hub Ottawa for their counsel and continued support. This research was funded by Carleton University and Bruyère Academic Medical Organization (BAMO) incentive fund grant.

VI. References

1. Versey, Z, et al. Biofilm-innate immune interface: Contribution to Chronic Wound Formation. *Frontiers in Immunology*, 2021*12*
2. Wolcott R, et al. Analysis of the CW microbiota….16S rdna pyrosequencing. *Wound Repair and Regen*, 2016*24*(1), 163–174.

Student: Rayhane Mejlaoui
Program: Master of Health Sciences
Co-Supervisors: Edana Cassol, Joerg Overhage

1st TEAM Hub Workshop
Ottawa, ON
June 26-28, 2023

TEAM Hub
Tissue Engineering & Applied Materials

Abstract - Understanding the effects of *Pseudomonas aeruginosa* biofilms on macrophage metabolism and function to improve wound care

R. Mejlaoui[1], Z. Versey[1], K. Allison[1], C. Beaulieu[1], Callen Lamourie[1], Duale Ahmed[1], Omar Abdo[1], K. deZeeuw[2], J. Marek[2], J. Overhage[1] and E. Cassol[1]

[1] Department of Health Sciences, Carleton University, Ottawa, Canada
[2]Saint-Vincent Hospital, Bruyère Research Institute, Ottawa, Canada

I. Introduction

Chronic wounds are a growing problem that can severely impact the quality of life of at-risk populations such as the elderly, and individuals with impaired mobility and coexisting conditions. One of the most significant barriers to wound healing is the presence of bacterial biofilms, which can develop antibiotic resistance and evade the immune system. Macrophages, as part of the innate immune system, play a critical role in the host defense against biofilm infections, including Pseudomonas aeruginosa biofilms. These macrophage functions They. However, the mechanisms by which *P. aeruginosa* biofilms modulate macrophage metabolism and function remain poorly understood. This study aims to investigate the effects of *P. aeruginosa* biofilms on macrophage metabolism and function and explore potential therapeutic strategies to improve wound care.

II. Methodology

Objectives: Develop mitochondrial and activation profiles associated with biofilm supernatants obtained from different *P. aeruginosa* strains (PAO1, CI5523).

Ex-vivo: Bone marrow derived macrophages obtained from young female mice were cultured and treated with *P. aeruginosa* biofilm supernatants. Cytokine levels were analyzed via ELISA and cell function markers were analyzed on an Attune Flow Cytometer.

In-vivo: Future steps include analyzing debridement and blood samples from a clinical human study in partnership with Saint Vincent Hospital.

Using a variety of sample sources including mouse macrophages and human samples has the benefit of being more representative of real patient wounds.

III. Results

Our results demonstrate that sustained exposure to biofilm supernatants from a clinical isolate and a lab strains of *P. aeruginosa* results in macrophage death.

Macrophage death following biofilm supernatants exposure may be a result of an acute increase in mitochondrial ROS and loss of mitochondrial membrane potential (Fig. 1).

P. aeruginosa biofilm supernatants also induce a strong early inflammatory response in macrophages that may subside over time.

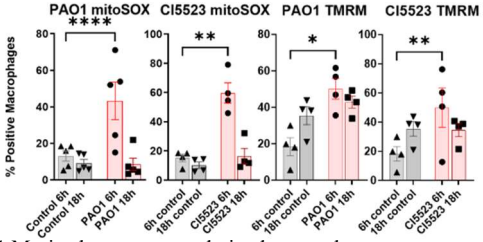

Fig. 1 Murine bone-marrow-derived macrophages were treated with 10^7 CFU/mL PAO1 or CI5523 biofilm supernatant at 6h and 18h.

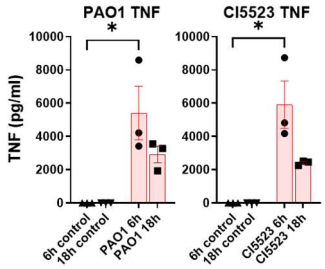

Fig. 2 Murine macrophages were treated with 10^7 CFU/mL biofilm supernatant at 6h and 18h. ELISA was performed.

IV. Conclusions

P. aeruginosa biofilm supernatants induced mtROS production, loss of mitochondrial membrane potential and inflammatory cytokine production in mouse macrophages. PAO1 results in similar macrophage mitochondrial activation and inflammation profiles as CI5523. A clinical Human Study in partnership with St-Vincent Hospital is in progress (n=4) for next steps. Chronic wounds are a growing problem especially with the ageing population in Canada. I hope to discover mechanisms that we can target in the future to restore wound healing.

Acknowledgements

Thank you to members of the Cassol and Overhage labs for their help. Thank you to our research partners, clinicians and support staff at Saint-Vincent Hospital and Bruyère Research Institute.

References

1. S. Z. Mordiffi, B. Kent, N. M. Phillips y G. K. C. Huat, "Assessing pressure injury risk using a single mobility scale in hospitalised patients: a comparative study using case-control design," Journal of Research in Nursing, vol. 23, no. 5, 2018, pp. 387-403.
2. G. Zhao, M. L. Usui, S. I. Lippman, G. A. James, P. S. Stewart, P. Fleckman y J. E. Olerud, "Biofilms and Inflammation in Chronic Wounds," Advances in Wound Care, vol. 2, no. 7, 2013, pp. 389–399.

1st TEAM Hub Workshop
Ottawa, ON
June 26-28, 2023

TEAM Hub
Tissue Engineering & Applied Materials

Elucidating the role of Schwann cell development in mesenchymal Tuberous Sclerosis Complex

Ella Wiljer[1,2], J. Yockell-Lelievre[1], W. Batoff[1], A. Pietrobon[1], William Stanford[1,2].
[1]Regenerative Medicine Program, The Ottawa Hospital Research Institute, Ottawa, Canada
[2]Department of Biochemistry Immunology and Microbiology, University of Ottawa, Ottawa, Canada

Introduction

Tuberous Sclerosis Complex (TSC) is a genetic multi-system neoplastic disease caused by mutations in the genes *TSC1* or *TSC2* [1]. Mesenchymal TSC (M-TSC) manifestations, Renal Angiomyolipoma (R-AML) and Lymphangioleiomyomatosis (LAM), are leading causes of TSC mortality. Development of effective therapeutics has been limited by a lack of biologically relevant preclinical models and the unknown cell origin of M-TSC. Recent findings from the Stanford Lab implicate a Schwann cell lineage-derived origin of M-TSC [2].

This project aims to unravel the molecular mechanisms through which mTOR-mediated Schwann cell fate determination informs development of surrounding tissues in the context of M-TSC pathogenesis.

Methodology

Stem cell-derived models of M-TSC: This work makes use of a novel renal organoid model of R-AML developed by directed differentiation of CRISPR/Cas9 engineered *TSC1/2*$^{-/-}$ human pluripotent stem cell (hPSC) lines in the Stanford lab [2]. Additional differentiation experiments using the in-house *TSC2*$^{-/-}$ hPSCs produce a novel *TSC2*$^{-/-}$ Schwann cell precursor (SCP) line.

Immunostaining: Immunofluorescence (IF), immunohistochemistry, and high content imaging are used identify aberrant Schwann cell expression and development in the *TSC2*$^{-/-}$ renal organoids, and to validate and characterize the *TSC2*$^{-/-}$ SCP lines.

scRNA-seq analyses of human M-TSC datasets: Differential analysis of intercellular communication is performed in renal organoid transcriptomic data using the R-based CellChat algorithm [3]. To assess M-TSC associated SC dysregulation, human LAM and R-AML patient scRNA-seq datasets [4,5] are parsed for SC lineage expression.

Results

R-AML associated SC-like populations in renal organoids: Findings of IF experiments show differential expression of SC markers, and co-localization with R-AML markers, in *TSC2*$^{-/-}$ end-stage renal organoids relative to WT. Bioinformatic analyses of renal organoid scRNA-seq data reveal global dysregulation of intercellular signaling networks in *TSC*-null relative to WT cells.

R-*AML-specific SC expression in human kidneys:* Data mining efforts using publicly available R-AML patient and healthy kidney datasets identify R-AML disease cell-specific expression of SC biomarkers.

Generating a novel developmental M-TSC cell model: I demonstrate proof of concept of a novel *TSC2*$^{-/-}$ Schwann cell precursor line as a promising method of modeling M-TSC *in vitro* and *in vivo*.

Conclusions

Here, we present evidence that that loss of *TSC2* induces dysregulation of Schwann cell fate trajectory in an *in vitro* model of kidney development. We identify an abnormal population of Schwann cell-like cells that express R-AML disease features in human M-TSC kidneys. We further provide proof of concept of a novel Schwann cell precursor cell model of M-TSC development. The significance of this ongoing project lies in its potential to generate multiple biologically relevant preclinical models that will provide a foundation for development of more effective and targeted therapeutics of M-TSC.

Acknowledgements

We thank the Stanford Lab for their insights and support, and The Ottawa Hospital Research Institute Stem Cell Core for their continued guidance and assistance.

References

1. Napolioni, V. & Curatolo, P. Genetics and Molecular Biology of Tuberous Sclerosis Complex. Current Genomics 9, 475-487 (2008).
2. Pietrobon, Adam, et al. Renal Organoid Modeling of Tuberous Sclerosis Complex Reveals Lesion Features Arise from Diverse Developmental Processes. Cell Reports, vol. 40, no. 1 (2022).
3. Jin, Suoqin et al., Inference and analysis of cell-cell communication using CellChat. Nature Communications, 12:1088 (2021).
4. Du Y et al., Lymphangioleiomyomatosis (LAM) Cell Atlas. Thorax 78(1):85-87 (2023).
5. Liao, J. et al. Single-cell RNA sequencing of human kidney. Sci Data 7, 4 (2020).

1st TEAM Hub Workshop
Ottawa, ON
June 26-28, 2023

TEAM Hub
Tissue Engineering & Applied Materials

An investigation into impact and strain-linked changes to the synapses in *ex vivo* porcine brain tissues

Gia Kang[1], Hannah Thomson[1], Brendan Hoffe[2], Rohan Banton[3], Thuvan Piehler[4], Matthew Holahan[2], Oren E. Petel[1]

1 Department of Mechanical and Aerospace Engineering, Carleton University, Ottawa, ON, Canada
2 Department of Neuroscience, Carleton University, Ottawa, ON, Canada
3 U.S. Army Research Laboratory, Aberdeen Proving Ground, MD, USA
4 U.S. Army Medical Research and Development Command, Fort Detrick, MD, USA

Introduction

The link between strain thresholds and the onset of brain tissue-level changes, particularly structure-specific strain thresholds for Mild Traumatic Brain Injury (mTBI), remains a pressing knowledge gap in the field of injury biomechanics. Prior work has demonstrated that the sulcus regions of the outer cortex are particularly susceptible to impact-induced microstructural changes [1], due to strain localization effects in a gyrencephalic brain [2]. In the present study, the response of the synapses following an impact event was investigated to determine, relating in overall spine density and dendritic spine types to strain levels.

Methodology

Porcine heads were collected from a local abattoir following sacrifice, their brains extracted, then sectioned into a set of coronal slabs (two control and two impact) using a brain slicing matrix. Each slab was instrumented with radio-opaque markers to track tissue deformation during impact and placed within an elastomer encasement [1,2]. The slabs, contained within their elastomeric encasements, were dropped onto a steel anvil from a height of 0.9 m. All impacts were imaged using a high-speed in situ X-ray cinematography system at 7,500 fps. Motion patterns of the individual markers were tracked via a feature-point particle tracker and used to calculate Maximum Principal Strain (MPS), Minimum Principal Strain (mPS) and Maximum Shear Strain. The slabs were taken for Golgi-cox staining and tested within one-hour post-impact. The strain response in different regions within the cortex were mapped out for each brain slab and compared to outcomes in overall spine density and spine type proportions.

Results

Results are shown in Figure 1 for the apical dendritic spine morphology type plotted against the peak tensile, compressive, and shear strains for five impacted coronal brain slabs. The plots highlight in slab comparisons among various cortical locations in both the gyrus and sulcus regions, as baseline spine type distributions may differ between individual brains. The control brain slabs in comparison, contained apical dendrite mushroom type values of 34.6 ± 1.5% and 33.5 ± 1.5% in the arm and apex locations respectively.

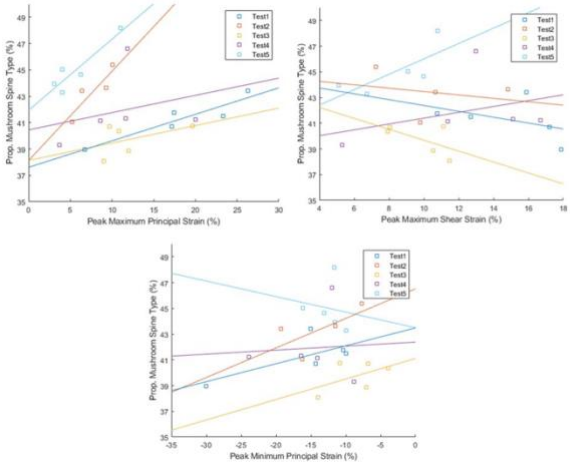

Fig. 1 Proportion of mushroom type spines in the apical layer of impacted porcine coronal slabs measured 1-hour post-impact compared to peak Maximum Principal Strain (tensile).

Conclusions

While the overall spine density did not change between control and impacted slab, the spine-type proportions varied between control and impacted slab. The apical and basal dendrites post-impact tended to shift into mushroom type spines in both arm and apex regions ($p < 0.05$) when comparing the control and impacted slabs. These results demonstrate that spines that were available to change, shifted towards mushroom spine types which are an excitatory spine type. The trends in Figure 1 illustrated that the apical dendritic morphology changes were sensitive to tensile loads (MPS), with mushroom-type morphologies becoming more prevalent with increasing MPS values for in-tissue comparisons. In contrast no clear trends were observed for compressive (mPS) or shear strains.

Acknowledgements

This work was supported under contract W911F-17-2-0222.

References

[1] Hoffe, B. et al. (2021) *Journal of Biomechanics*, 128, 110708.

[2] Mazurkiewicz, A. et al. (2021) *Journal of Biomechanical Engineering*, 143(6), 061015.

1st TEAM Hub Workshop
Ottawa, ON
June 26-28, 2023

TEAM Hub
Tissue Engineering & Applied Materials

An *in vitro* model of articular cartilage incorporating a calcified zone

M.S. Mulholland[1], M. Pickell[2], S. Carsen[3], F. Variola[4] and J.-P. St-Pierre[1]

[1]Department of Chemical and Biological Engineering, University of Ottawa, Ottawa, Canada
[2]Department of Surgery, The Ottawa Hospital, Ottawa, Canada
[3]Division of Orthopedics, Children's Hospital of Eastern Ontario, Ottawa, Canada
[4]Department of Mechanical Engineering, University of Ottawa, Ottawa, Canada

Introduction

Osteoarthritis is a debilitating illness experienced by an estimated 5 million Canadians, whose symptoms include joint pain and loss of range of motion[1]. There is currently no cure or disease-modifying drug to halt or reverse its progression. A hallmark of osteoarthritis in its early stages is the thickening of the calcified zone of articular cartilage, believed to be caused by imbalances in metabolic processes controlling mineralization, which are not well understood[2]. It is therefore the focus of this project to establish an in vitro model, which may be used to study mineralization in articular cartilage.

Methodology

Deep zone cartilage was harvested from the metacarpophalangeal joint of young cows within 24 hours of death. Tissue was digested enzymatically to yield a suspension of deep zone chondrocytes, which were seeded at high density onto tissue culture membrane inserts. Based on previous work, cells were cultured in mineralization media, notably comprising β-glycerophosphate to promote cell-driven mineralization. At two-week intervals grown tissues were harvested for analysis, up to a total of eight weeks. Tissues were fixed in formalin and stained with Von Kossa to discern the mineral phase, with a Hematoxylin counterstain. Another set of tissues was decalcified for eight weeks in EDTA and stained with safranin-O to show the structure of underlying matrix in the mineral phase. Additional fixed tissues were characterized using confocal Raman spectroscopy to quantify mineral-to-matrix ratio, crystallinity, and carbonate substitution. Mineral in tissues was also quantified by dissolving tissues in HCl and assaying for calcium and phosphate content.

Results

Histological stains revealed that a calcified zone forms in the deepest aspect of the tissue, along the membrane. Individual mineral deposits visible at two weeks form a uniform layer at approximately four weeks, which continues to grow up to eight weeks. This is supported by assays for calcium and phosphate, which indicate that mineral continues to deposit up to at least eight weeks in culture. Raman spectra collected in the mineral phase of tissue shows a prominent peak at ~960cm-1, attributed to the symmetric stretching vibration $\nu_1(PO_4^{3-})$. Calculating the area ratio of the phosphate band and the amide I band at ~1650cm^{-1} yields an estimate of the mineral-to-matrix ratio, which is seen to increase over the course of the study. Comparison with native tissue spectra revealed that after four weeks, the mineral-to-matrix ratio rises above that found in native calcified cartilage. Similarly using the intensity ratio of the $\nu1(PO_4^{3-})$ band to the carbonate $\nu_1(CO_3^{2-})$ peak at ~1070 cm-1, the degree of carbonate substitution is observably lower than in reference native tissue.

Conclusions

Results from the time course study indicate that for these conditions, a stable mineral phase is not achieved by eight weeks. This is evidenced by calcium assay and supported by Raman spectroscopy data, which show that at four weeks, matrix deposition is outpaced by mineralization. This is suggested to occur because the βGP concentration used is much higher than physiological levels. Future experiments will be designed around finding culture conditions which maintain a stable mineral phase, perhaps after the initial layer has formed. Bringing the model to equilibrium in this way will aid in the study of calcification by allowing the investigation of culture factors which cause deviations from steady state.

Acknowledgements

We would like to acknowledge the support of all our lab colleagues in the St-Pierre Biomaterials Group. For training and assistance with Raman spectra acquisition we thank Alex Steeves and the rest of the Variola Research Group. We would also like to acknowledge the contribution of the Louise Pelletier Histology Core Facility at the University of Ottawa in their preparation of histological stains for this project.

References

[1] "Osteoarthritis - Symptoms, Causes, Diagnosis & Treatments." [Online]. Available: https://arthritis.ca/about-arthritis/arthritis-types-(a-z)/types/osteoarthritis

[2] B. M. Daubs, M. D. Markel, and P. A. Manley, "Histomorphometric analysis of articular cartilage, zone of calcified cartilage, and subchondral bone plate in femoral heads from clinically normal dogs and dogs with moderate or severe osteoarthritis," *ajvr*, vol. 67, no. 10, pp. 1719–1724, Oct. 2006, doi: 10.2460/ajvr.67.10.1719.

1st TEAM Hub Workshop
Ottawa, ON
June 26-28, 2023

TEAM Hub
Tissue Engineering & Applied Materials

Development of Inorganic Polyphosphate-Based Nanoparticles for Drug Delivery into Articular Cartilage

Jordan Nhan[1], Nicolas Strebel[1], Khushnouma Virah Sawmy[1], Jordan Yin[1] and Jean-Philippe St-Pierre[1]

[1]Department of Chemical and Biological Engineering, Faculty of Engineering, University of Ottawa, Ottawa, ON, Canada

Introduction

Osteoarthritis (OA) is the most common form of arthritis, characterized by the progressive loss of articular cartilage. Currently, no drugs have been approved to stop the progression of OA, and rather focus on the management of symptoms. This is partly due to the many challenges in the delivery of drugs to afflicted joints. As cartilage is avascular, intra-articular injections may be performed for the local administration of drugs into the joint capsule, however small molecules are rapidly cleared from the synovial fluid within hours. Furthermore, AC has a dense extracellular matrix (ECM) composed of collagens and proteoglycans, which can act as a physical barrier for biomolecule entry. Therefore, there is a need to develop effective drug delivery techniques to improve both the residence time within the joint, as well as cartilage tissue penetration capabilities, which may be accomplished by nanoparticle-based drug carriers. Previous studies have identified polyphosphate (polyP) as a molecule of interest, promoting ECM accumulation in engineered cartilage tissues, which may reverse the degeneration of cartilage observed in OA [1]. For this purpose, we have synthesized and characterized strontium-polyphosphate (Sr-polyP) particles as a potential drug delivery method into cartilage.

Methodology

Sr-polyP particles were synthesized by dropwise addition of polyP to a strontium crosslinking bath under agitation and maintained at a pH of at least 10 for 3 hours. The size of the as synthesized or sonicated particles in DMEM with or without serum supplementation was measured by dynamic light scattering (DLS) and zeta potential was also measured under the same conditions. Scanning electron microscopy (SEM) was performed to visualize particle shape and morphology. Cellular uptake of DAPI-stained Sr-polyP particles in primary bovine chondrocytes was confirmed through fluorescent microscopy. Live-dead, MTT, and EdU assays were also performed to assess cell viability, metabolic activity, and cell proliferation respectively. Cartilage tissue penetration was confirmed by fluorescent imaging of bovine cartilage explants incubated with DAPI-stained Sr-polyP particles.

Results

Sr-polyP particles have a negative zeta potential ($\zeta = -12.9 \pm 0.8$ mV) and poor size stability in DMEM due to its high osmolarity, resulting in particle agglomeration (Z-average > 2000 nm). Supplementation of 10% FBS improved size stability as a result of protein adsorption, maintaining a Z-average between 230 – 300 nm over 4 days. Intracellular uptake of Sr-polyP was confirmed in chondrocytes (Fig. 1), and cytotoxicity was determined to be both size- and concentration-dependent. MTT and EdU assays indicated a reduction in metabolic activity and cell proliferation. Furthermore, preliminary results suggest that the particles may penetrate and be retained in native cartilage explants.

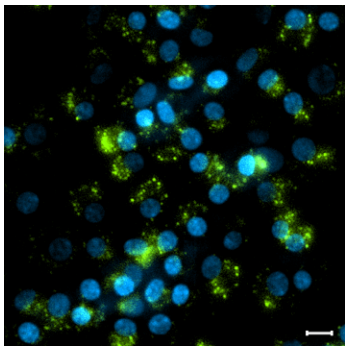

Fig. 1 Cellular uptake of Sr-polyP particles. Particles (green) and nuclei (blue) are both stained with DAPI. Scale bar = 20 µm.

Conclusions

This study aims to develop a nanoparticle-based drug carrier utilizing polyP to stimulate ECM accumulation and improve residence times in the joint. Our results indicate that Sr-polyP particles are suitable for chondrocytes in vitro as observed by successful uptake, high cell viability, and a reduction in cell proliferation which may indicate a role in maintaining the chondrogenic phenotype. Changes in metabolic activity were also observed as expected, due to polyP having a role in bioenergetics and metabolism.

Acknowledgements

JN received an NSERC CGS-M and an OGS award. This study was funded by NSERC with equipment acquired with CFI-JELF funds and matching funds from the Ministry of Economic Development, Job Creation and Trade Ontario Research Fund. JPS also received support from the Arthritis Society Canada.

References

1. J.-P. St-Pierre, Q. Wang, S. Q. Li, R. M. Pilliar, and R. A. Kandel, "Inorganic Polyphosphate Stimulates Cartilage Tissue Formation," *Tissue Eng Part A*, vol. 18, pp. 1282–1292, 2012.

1st TEAM Hub Workshop
Ottawa, ON
June 26-28, 2023

TEAM Hub
Tissue Engineering & Applied Materials

Detection of Radar-based Human Fall Events as Anomalies

Ankita Dey[1*], Sreeraman Rajan[1**], Gaozhi Xiao[2] and Jianping Lu[2]

[*] Student pursuing PhD in electrical and computer engineering, [**]PhD Supervisor
[1]Department of Systems and Computer Engineering, Carleton University, Canada, [2]National Research Council (NRC), Canada

Introduction

Fall is a concern worldwide due the ageing population as it may lead to hospitalization, permanent disability or even death in extreme cases. As steps toward fall prevention, it is necessary to understand and detect falls. Radar-based sensing for human activity recognition including falls has been a growing area of research as radars are contactless and privacy preserving. Currently, state-of-the-art deep learning models widely used for fall event detection are trained on large number of simulated fall and non-fall samples. However, in real-life scenario, falls are rare anomalies, and the number of fall training samples are very few. Artificial data augmentation techniques generally do not mimic real life scenarios and hence technology transfer from lab to market is in its gestation stage. Thus, developing techniques that can detect a fall event as an outlier is crucial. This abstract proposes a novel one-class classification (OCC) framework that uses only non-fall samples for training and detects falls as an anomaly. This work pioneers the application of anomaly detection techniques in the field of radar-based fall event detection. The model proposed in this work fuses features obtained from pre-trained models which are then used for anomaly detection using unsupervised OCC models for classification [1].

Methodology

A publicly available recent dataset released by University of Glasgow [2] is considered for evaluation. 60 participants performed 5 different daily life activities and simulated falls at 3 different locations. A total of 1164 complex temporal series (fall and non-fall) are used in this work. Fig. 1 shows the proposed feature fused fall anomaly detection pipeline which is elaborated as:

Step-1: The complex temporal series are arranged into radar data matrix and short-time Fourier transform was applied on this data matrix to form time-frequency (TF) representation (spectrograms); **Step-2:** The spectrogram images are fed into pre-trained models, namely, VGG16, VGG19 and EfficientNet B0 (ENB0), to extract abstract features; **Step-3:** The abstract features are fused (or concatenated) to form fused feature space; and **Step-4:** The fused feature space is fed into OCC models, namely, one-class support vector machine (OC-SVM), Isolation Forest (IF) and Local Outlier Factor (LOF) for anomaly (or fall) detection.

Results

Due to the presence of highly imbalanced data, the performance of anomaly detection algorithms is evaluated using ROC-derived metrics such as area under ROC curve (AUC) and half total error rate (HTER). The results obtained are shown in Table.1. LOF algorithm outperforms OSVM and IF algorithms at all testing locations irrespective of the features used. LOF using fused feature space of ENB0+VGG-19 provides the best fall event classification at all testing locations.

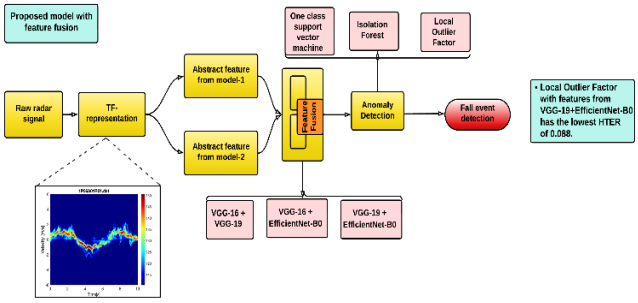

Fig. 1 Proposed feature fused fall anomaly detection pipeline.

Table 1 - Performance metrics of various OCC with different combined pre-trained model features for different location testing.

Loc	Testing location A			Testing location B			Testing location C		
Feature	OSVM	IF	LOF	OSVM	IF	LOF	OSVM	IF	LOF
VGG-16+ VGG-19	HTER = 0.24 AUC= 0.75	HTER = 0.21 AUC= 0.78	HTER = 0.19 AUC= 0.80	HTER = 0.12 AUC= 0.87	HTER = 0.17 AUC= 0.85	HTER = 0.09 AUC= 0.90	HTER = 0.27 AUC= 0.72	HTER = 0.32 AUC= 0.67	HTER = 0.10 AUC= 0.90
ENB0 + VGG-16	HTER = 0.23 AUC= 0.76	HTER = 0.24 AUC= 0.75	HTER = 0.19 AUC= 0.80	HTER = 0.12 AUC= 0.87	HTER = 0.14 AUC= 0.85	HTER = 0.10 AUC= 0.89	HTER = 0.27 AUC= 0.72	HTER = 0.30 AUC= 0.69	HTER = 0.09 AUC= 0.90
ENB0 + VGG-19	HTER = 0.22 AUC= 0.77	HTER = 0.22 AUC= 0.78	HTER = 0.18 AUC= 0.81	HTER = 0.12 AUC= 0.87	HTER = 0.15 AUC= 0.84	HTER = 0.09 AUC= 0.90	HTER = 0.17 AUC= 0.82	HTER = 0.26 AUC= 0.73	HTER = 0.08 AUC= 0.91

Conclusions

This work pioneers the application of one-class classification techniques using fusion of two feature spaces for radar-based fall event detection systems. As future work, one-class classification with different types and orientations of radars along with different radar domains will be studied.

Acknowledgements

This work was financially supported by the Aging in Place Challenge Program at National Research Council of Canada (NRC).

References

1. A. Dey, S. Rajan, G. Xiao and J. Lu, "One-class Classification for Radar-based Human Fall Event Detection," in IEEE Sensors Letters, doi: 10.1109/LSENS.2023.3284652.
2. F. Fioranelli, S. A. Shah, H. Li, A. Shreshtha, S. Yang, and J. Kernec, "Radar sensing for healthcare," Electronics Letters, vol. 55, no. 19, pp. 1022–1024, 2019.

1st TEAM Hub Workshop
Ottawa, ON
June 26-28, 2023

Elucidating the Lipidomic Dynamics of Lentiviral Production and Infection

Joshua A Roberts[1,5], Elena Godbout[3], Christopher Boddy[2], Jean-Simon Diallo[3,4], Jeffrey C Smith[1,5]

[1]Department of Chemistry, Carleton University, Ottawa, Canada
[2]Department of Chemistry and Biomolecular Sciences, University of Ottawa, Ottawa, Canada
[3]Ottawa Hospital Research Institute, University of Ottawa, Ottawa, Canada
[4]Virica Biotech Inc, Ottawa, Canada
[5]Carleton Mass Spectrometry Centre, Carleton University, Ottawa, Canada

Introduction

Lentiviral vector (LV) therapies are emerging as sophisticated and effective bio-therapeutics for treating immunodeficiencies and cancer. Clinical-grade LV production for therapeutic use is extremely expensive, requiring specialized packaging cells and bioreactor technology to produce harvestable quantities of virus to treat a single patient. The lipid dynamics of producing LV in this setting are poorly understood. Reports from the closely related human immunodeficiency virus (HIV) have shown that altering its lipid composition throught treating the producer cells with Fumonisin B1 lowers transducibility by inhibiting ceramide and sphingomyelin synthesis. This suggests that the composition of the lipid envelope is critical for transduction. Understanding the lipid dynamics of producing LV may improve the quality and yield of LV from a biomanufacturing context..

Methodology

HEK 293T cells were cultured in 6-well plates and transfected with LV production plasmids and the single Vesicular stomatitis virus G (VSVG) plasmid followed by 48 hours incubation. To analyze the lipidome of LV, HEK293T cells were cultured in two T75 flasks producing LV or in plain culture media for 48 hours, LV was purified from media by ultracentrifugation. Lipids were extracted using a modified Bligh-Dyer protocol and analyzed by mass spectrometry (MS) using an Agilent 6546 QTOF. Lipids were identified from tandem MS (MS/MS) data using Agilent Lipid Annotator and were then extracted using MZmine 2. Samples were normalized using Normalyzer (http://normalyzer.immunoprot.lth.se/-index.php) and missing values were imputed using MetImp (https://metabolomics.cc.hawaii.edu/software-/MetImp). R and Microsoft Excel were used for statistical analysis.

Results

After producing LV for 48 hours, widespread depletion of lipids from phosphatidylinositol, phosphatidylcholine and sphingomyelin classes was observed.Triacylglycerols and ether-linked phosphatidylethanolamines and phosphatidylcholines were found to increase in abundance in the LV-producing HEK 293T cells compared to controls. LV titers were determined to be 1.25E6 TU/mL after 48 hours. HEK 293T cells were also examined for metabolic activity using a resazurin assay and found to be 94% active compared to controls, indicating they were healthy despite 48 hours of LV production. Production of the lone VSVG protein by HEK 293T was used as a control to determine any lipidomic changes as a result of exosome secretion, for which there is previous evidence for. VSVG production resulted in no observable change to the HEK 293T lipidome compared to control cells. Using Agilent's Lipid Annotator, 300 unique lipids from 19 classes were identified in the concentrated LV fraction from the contents of two T75 flasks containing HEK 293T cells after 48 hours of LV production. Compared to concentrated media from untransfected cells, 160 lipids were uniquely found in media containing LV.

Conclusions

While previous reports from studying HIV showed the viral envelope consisted of mainly phosphatidylcholine, phosphatidylserine, phosphoinositol, sphingomyelin and free cholesterol, several instances of neutral lipids like diacylglycerols, cholesterol esters, and triacylglycerols were identified in the concentrated LV fraction. The exact source of these neutral lipids are currently unknown. Future work will investigate whether these lipids unique to the concentrated LV fraction are critical for LV transduction, and if disrupting the synthesis or remoldeling pathways of certain lipid classes affects the production or transduction of LV.

Acknowledgements

The authors would like to acknowledge NSERC and OGS for their support with funding.

References

1. Blood, 2000, 95 (8), 2499–2504.
2. Hum. Gene Ther. Methods, 2018, 29 (1), 1–15.
3. Gene Ther., 2018, 25 (1), 39–46.
4. PNAS, 2006, 103 (8), 2641-2646.
5. J. Vis. Exp., 2014, 91, e51890.

1st TEAM Hub Workshop
Ottawa, ON
June 26-28, 2023

TEAM Hub
Tissue Engineering & Applied Materials

Investigating Cellular Response to Mechanical Stretch Through Proximity Labeling Experiments

S. Desroches, D. Delgado, G. Kang, & A. Harris

MASc Biomedical Engineering Student, Department of Mechanical and Aerospace Engineering, Carleton University, Ottawa, Canada

Introduction

The cytoskeleton is a network of proteins responsible for cellular processes such as morphogenesis and motility [1]. These processes are often regulated via mechanical forces acting upon the cytoskeleton, which are then converted to cellular signals via mechanosensitive proteins [1]. A key relationship therefore exists between mechanical forces and cellular function. To improve our understanding of this relationship and determine which proteins are in fact mechanosensitive, a cell stretching system will be used in combination with proximity labeling to investigate changes in protein localization in response to various strain rates.

Methodology

Proximity labeling is a laboratory technique used to generate a proteomic map and therefore understand protein interactions which dictate cellular function [2]. A subcellular compartment of interest must first express an enzyme capable of catalyzing a labeling reaction with lysine side chains on all endogenous proteins located within a specified radius [2]. The enzyme responsible for catalyzing labeling reactions is referred to as TurboID, where biotin is then used as the labeling-substrate capable of tagging proteins within the specified radius [2]. The biotin-labeled endogenous proteins can then be identified using fluorescently tagged streptavidin via confocal imaging. Further analysis will also be completed using mass spectrometry to identify which proteins have been tagged. TurboID enzyme expression can be achieved via transient transfections using a HEK293T cell line.

A cell stretcher system will be used to stretch cells expressing the TurboID enzyme at various strain rates. Cells will be attached to a polydimethylsiloxane (PDMS) sheet, which will then be mounted onto the cell stretcher system and stretched, followed by the addition of biotin to initiate tagging. A stretched and unstretched sample will be compared to determine differences in protein localization, and therefore which proteins are impacted by these mechanical forces.

Results

Successful localization of the TurboID construct has been achieved in two different cellular locations including the nucleus and cytoplasm. Construct localization was achieved via transient transfection in a HEK293T cell line. Qualitative results are demonstrated in Figure 1 below, where the cell nuclei are represented by a DAPI signal and TurboID expression is represented by an AF 488 signal. Images were acquired using a Zeiss LSM 980 system.

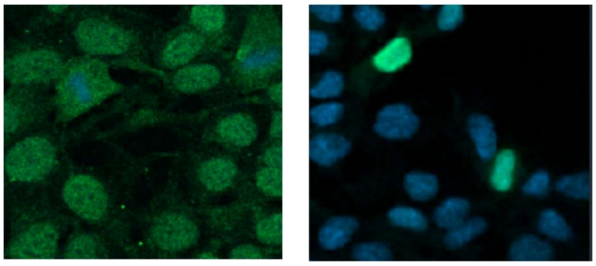

(a) (b)

Fig. 1 Successful TurboID enzyme expression in (a) the cytoplasm and (b) the nucleus.

Conclusions

Successful TurboID localization has been achieved to both nuclear and cytoplasmic regions via transient transfection. Future direction of this work will include adding a biotin labeling-substrate to cells expressing TurboID to tag all endogenous proteins surrounding the organelle of interest. Once this has been achieved, a stretched and unstretched sample will be compared to determine variation in protein localization and which proteins are therefore mechanosensitive. These findings will ultimately improve our understanding of cellular response to mechanical forces such as stretching.

Acknowledgements

The plasmids used in this work (V5-TurboID-NES_pCDNA3 & 3xHA-TurboID-NLS_pCDNA3) were deposited by The Alice Ting Lab at Stanford University (Addgene plasmid #107169 & #107171).

References

1. H. Belly, E. Paluch, and K. Chalut, “Interplay between mechanics and signaling in regulating cell fate,” Nat. Rev. Mol. Cell Biol, vol. 23, pp. 465-480, 2022.
2. T. Branon, J. Bosch, A. Sanchez, N. Udeshi, T. Svinkina, S. Carr, J. Feldman, N. Perrimon, and A. Ting. “Efficient proximity labeling in living cells and organisms with TurboID,” Nat. Biotechnol. Vol. 36, pp. 880-887, 2018.

1st TEAM Hub Workshop
Ottawa, ON
June 26-28, 2023

Inside-Out: Understanding aberrant expression of intracellular proteins at the cell surface during hypoxia

A.T. Star[1,2], A.S. Haqqani[2] and W.G. Willmore[1]

[1] Department of Biology, Carleton University, Ottawa, Canada
[2] Human Health Therapeutics, National Research Council of Canada, Ottawa, Canada

Introduction

Aberrant expression of intracellular proteins at the cell surface has the potential to identify new therapeutic targets in disease states. These novel targets would enable the development of highly-specific targeting of biotherapeutics to tissues experiencing stress, reduce toxicity to normal tissues, and increase therapeutic efficacy. Previous work has shown the translocation of some intracellular proteins, previously thought to be strictly cytosolic, to the cell surface under hypoxia where they can take on new roles in the extracellular environment [1]. We believe that a much wider variety of endoplasmic reticulum (ER) and other intracellular proteins may be present on the cell surface during cellular stress, despite their lack of a canonical secretory sequence. We hope to identify aberrantly expressed proteins on the cell surface during hypoxia in lung epithelial and fibroblast cells. This work will provide 1) novel therapeutic candidates for hypoxia related diseases, 2) insight into the roles played by these proteins in the hypoxic environment and 3) a better *in vitro* model for therapeutic target selection.

Methodology

Hypoxic exposure: A549 cells were incubated at 37ºC in 1% O_2 and 5% CO_2 overnight in the Baker/Ruskinn InvivO2 400 Hypoxic Workstation.
Cell surface isolation: The cells were washed with 1X PBS and were labeled with Sulfo-NHS-SS-Biotin. The reaction was quenched, followed by cell scraping and collection by centrifugation. The pellet was lysed with 1X RIPA followed by pulldown with streptavidin beads. The biotinylated cell surface proteins were released by reduction with DTT. The captured cell surface proteins and whole cell lysates were prepared for mass spectrometry by SP3 protocol.
Mass spectrometry: The samples were run on the Orbitrap Eclipse™ Tribrid™ mass spectrometer by DDA followed by PRM on proteins of interest.

Results

Cell surface enrichment: We have shown that we are able to enrich for proteins at the cell surface using Sulfo-NHS-SS-Biotin (Figure 1).

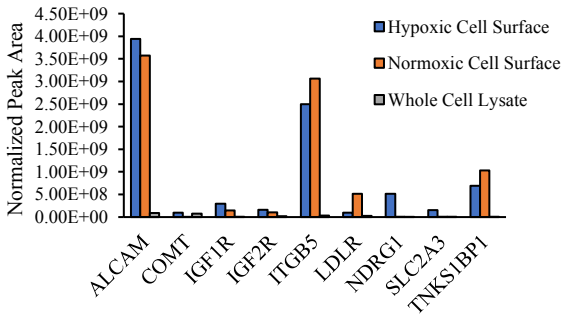

Fig. 1 Cell surface proteins are enriched in cell surface samples. N=1

Unexpected proteins at cell surface: Many ER proteins were also seen to be enriched at the cell surface in the cells exposed to hypoxic conditions.

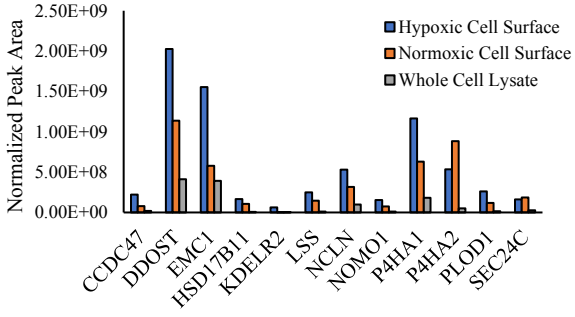

Fig. 2 ER proteins are enriched in hypoxic cell surface samples. N=1

Conclusions

Hypoxia causes aberrant proteins to be expressed at the cell surface.

Acknowledgements

We would like to acknowledge L. Tessier and S. Williamson from the mass spectrometry facility at the National Research Council of Canada and J. Hill for cell surface isolation advice and guidance.

References

1. Gonzalez-Gronow M, Selim MA, Papalas J, Pizzo SV. GRP78: a multifunctional receptor on the cell surface. Antioxid Redox Signal. 2009 Sep;11(9):2299-306. doi: 10.1089/ARS.2009.2568. PMID: 19331544.